Hindered settling of a log-normally distributed Stokesian suspension
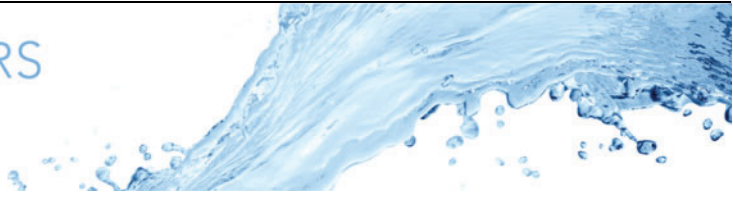
Li, H.; Botto, L.

Important note
To cite this publication, please use the final published version (if applicable).
Please check the document version above.

JM PAPERS

Hindered settling of a log-normally distributed Stokesian suspension

Heng Li[1] and Lorenzo Botto[1],†

[1]Process and Energy Department, ME Faculty of Mechanical Engineering, TU Delft, 2628 CD Delft, The Netherlands

Settling velocity statistics for dilute, non-Brownian homogeneous suspensions of polydisperse spheres having a log-normal size distribution are generated from Stokesian dynamics simulations, as a function of the total volume fraction ϕ and normalised width α of the particle size distribution. Several hundred instantaneous configurations are averaged to obtain reliable statistics. The paper reports data for the average and fluctuating settling velocity of each particle class in a suspension that is widely polydisperse – previous work was limited to only two or three classes, and the average settling velocity of each particle class was in most cases not reported – and provides an assessment of the accuracy of the analytical models proposed by Batchelor, Richardson & Zaki, Davis & Gecol and Masliyah–Lockett–Bassoon in predicting the simulation data. A limited comparison with dynamic simulations in which the particle microstructure is allowed to evolve in time is also included.

Key words: Stokesian dynamics, particle/fluid flow, suspensions

1. Introduction

Prediction of the settling velocity of polydisperse suspensions is crucially important in applications ranging from wastewater treatment (He *et al.* 2021) to nanoparticle sorting (Bonaccorso *et al.* 2013), particle size characterisation (Papuga, Kaszubkiewicz & Kawałko 2021) and sediment transport modelling (Dorrell & Hogg 2010). Despite decades of research on the settling of polydispersed suspensions this field still offers interesting scientific problems. A central challenge that this paper aims to address is the quantification of the settling velocity of each particle class in a suspension that is truly polydisperse, meaning that the number of classes exceeds the two or three classes

† Email address for correspondence: l.botto@tudelft.nl

that simulations (Revay & Higdon 1992; Cunha *et al.* 2002; Abbas *et al.* 2006; Wang & Brady 2015) and experiments (Al-Naafa & Selim 1992; Davis & Gecol 1994; Chen *et al.* 2023) have so far focused on. To quantify such velocity with high accuracy we perform Stokesian dynamics simulations, in the relatively dilute regime (solid volume fraction ϕ less than 0.1) for which phenomena of particle segregation and clustering are not expected to be very important; for $\phi \ll 1$, the theory of Batchelor (1982) for polydispersed suspensions should be sufficiently accurate and can be used to provide a framework for the analysis, hence the focus on the dilute regime. Furthermore, in addition to validating Batchelor's model for non-negligible volume fractions, this paper aims to assess the accuracy of the three most used one-dimensional models for the settling velocity of each class – the Davis & Gecol model, the Masliyah–Lockett–Bassoon (MLB) model and the polydisperse Richardson–Zaki model – in predicting the simulated settling velocity data as the particle concentration increases (these models are reviewed in § 2). There are claims in the literature that semi-empirical models that do not take into account the full particle size distribution, such as the MLB and the polydisperse Richardson–Zaki models, are able to capture accurately the sedimentation of a suspension. However, these models have not in fact been rigorously validated; only the ability to roughly capture concentration profiles for selected parameters has been checked. Therefore it seems important to validate these models which are routinely used in practical settings (Berres, Bürger & Tory 2005; Dorrell & Hogg 2010). If such models do predict the settling velocity of some particle classes, we would like to know for which particle range they provide accurate predictions and with what error.

The particle size distribution is assumed to be a log-normal one. The log-normal particle size distribution is ubiquitous in particulate systems, and the accurate prediction of the class-averaged particle velocity for log-normally distributed particles has recently become important because of the need for accurate size fractionation of micro- and nanoparticles (Bonaccorso *et al.* 2013; Backes *et al.* 2016).

Despite recent interest in the modelling of suspensions of wide and continuous size distributions (Pednekar, Chun & Morris 2018; Gonzalez, Aponte-Rivera & Zia 2021; Howard, Maxey & Gallier 2022; Malbranche, Chakraborty & Morris 2023; Lavrenteva, Smagin & Nir 2024), data on the settling of polydisperse suspensions with many size classes are surprisingly scarce. Physical experiments have been mostly carried out for bidisperse or tridisperse suspensions (Lockett & Bassoon 1979; Davis & Birdsell 1988; Al-Naafa & Selim 1992; Davis & Gecol 1994; Chen *et al.* 2023). The largest size ratio between two size classes considered in these experiments was about 4, and only the velocity of the largest size class was, in some experiments, measured (strictly speaking, in these experiments the velocity of the interface between different quasi-homogeneous particulate regions was measured, not the actual particle velocity). Numerical simulations have been carried out for bidisperse suspensions using Stokesian dynamics (Revay & Higdon 1992; Cunha *et al.* 2002; Wang & Brady 2015) and the force coupling method (Abbas *et al.* 2006), with size ratios up to 4. In these simulations the velocity of each particle class was measured and compared with model predictions. Simulations of sedimentation of suspensions with a continuous log-normal distribution have been carried out by Vowinckel *et al.* (2019) in a domain bounded by top and bottom walls, but in that study the velocity of each size class was not quantified. There is a wealth of interesting data on sedimentation of polydisperse suspensions from the geophysical literature (Cuthbertson *et al.* 2008; Spearman & Manning 2017). However, these data are often difficult to interpret from a fluid mechanic perspective, as the particulate systems considered in those references are usually heterogeneous in particle shape and material properties, and the particle–particle interactions are not only hydrodynamic in nature.

Particle velocity statistics in the current paper are calculated for polydisperse suspensions of non-Brownian, inertialess, low-Reynolds-number spheres of uniform mass density, having discrete particle size classes that are fitted to continuous log-normal distributions for different values of the polydispersity parameter α (see figure 4), defined as the ratio between the standard deviation and the mean value of the particle size distribution. The size distribution is chosen to be a log-normal one because of the recurring presence of this distribution in polydispersed particle systems (Vowinckel *et al.* 2019; Di Vaira *et al.* 2022; Rettinger *et al.* 2022). The log-normal size distribution is discretised into up to nine classes, with the largest size ratio between two classes being 5 (see figure 4). We vary the volume fraction ϕ from 0.01 to 0.1 and α in the range 0.1–0.4. As a base case we include in § 4 data for mono- and bidisperse suspensions, for which some literature information is available. In addition to mean particle velocities, the corresponding standard deviations and the shape of the particle velocity distributions are reported. This information provides a quantitative characterisation of the spread of the particle velocity around the mean as the polydispersity in particle size is increased.

To be able to compare against theoretical models, producing smooth data not affected by large statistical error is essential. This constraint has required us to average the velocity data over hundreds of simulations. To keep the simulation cost manageable while allowing us to explore a range of relevant parameters of solid concentration and polydispersity, following other authors (Revay & Higdon 1992; Cunha *et al.* 2002; Abbas *et al.* 2006; Wang & Brady 2015), we produce converged particle velocity statistics by generating a large number of random particle configurations inside a triply periodic box, and ensemble-averaging over all such configurations. Despite limitations, which are discussed in § 6, this established approach has in the past enabled fundamental insights into the relation between particle concentration and settling rate (see e.g. Wang & Brady 2015). In § 6 we compare, for selected parameters, random array simulations to dynamic simulations in which the particle microstructure is allowed to evolve in time. Differences between the two simulation approaches have been found not so large to affect the main conclusions of the paper.

2. Overview of one-dimensional models for the class-averaged settling velocity

For a Stokesian suspension of polydisperse spheres grouped into m distinct particle size classes, the average settling velocity of the ith class can be written as $\langle u_i \rangle = u_{St,i} h_i(\boldsymbol{\phi})$, where $u_{St,i} = (2/9\mu) a_i^2 (\rho_p - \rho_f) g$ is the single-particle Stokes velocity of the ith class, $h_i(\boldsymbol{\phi})$ is the hindered settling function of that class and $\boldsymbol{\phi} = (\phi_1, \phi_2, \ldots, \phi_m)$ is the vector of volume fractions (Davis & Acrivos 1985); a_i is the particle radius, μ is the fluid viscosity and $\rho_p - \rho_f$ is the density difference between the particles and the fluid.

The literature reports several models for $h_i(\boldsymbol{\phi})$, as reviewed by Berres *et al.* (2005). The only model that is completely based on first principles is the model of Batchelor (1982), which was developed as an extension of the former theory of Batchelor for monodisperse suspensions (Batchelor 1972). Batchelor's formula reads

$$h_i(\boldsymbol{\phi}) = 1 + \sum_{j=1}^{m} S_{ij}\phi_j, \tag{2.1}$$

where S_{ij} are scalar sedimentation coefficients that are functions of the size ratio a_i/a_j for spheres of identical mass density (Batchelor & Wen 1982) (an explicit expression for S_{ij} is given in § 5.2). Batchelor's model is accurate to first order in the total volume fraction

$\phi = \sum_j \phi_j$ and is, therefore, in principle only valid for negligibly small values of ϕ. A semi-empirical extension of Batchelor's formula was proposed by Davis & Gecol (1994) to improve the predictive capability in the regime of relatively high volume fractions. Their formula reads

$$h_i(\boldsymbol{\phi}) = (1 - \phi)^{-S_{ii}} \left(1 + \sum_{j=1}^{m} (S_{ij} - S_{ii}) \phi_j \right), \qquad (2.2)$$

where the coefficients S_{ij} are defined as in (2.1). The model is essentially an interpolation formula between an exact result (for $\phi \to 0$, (2.2) recovers (2.1)) and an approximate result (in the dense limit, for $m = 1$ equation (2.2) reduces to a power-law form, where the exponent $-S_{ii} = 6.55$ is numerically close to the exponent $\simeq 5$ of the well-known Richardson–Zaki formula). The models of Batchelor and Davis & Gecol have been tested in experiments and simulations of bidisperse suspensions (Davis & Birdsell 1988; Al-Naafa & Selim 1992; Abbas *et al.* 2006; Wang & Brady 2015; Chen *et al.* 2023). In experiments, the descending velocities of the interfaces separating different regions were measured. In simulations, settling velocities of the two classes were calculated. It was shown that Batchelor's model works reasonably well for dilute suspensions with ϕ within 5 %, and Davis & Gecol's model can also be used for dense suspensions.

Models (2.1) and (2.2) are rarely used in practice because they contain a large number of coefficients. Simpler expressions have therefore been developed for practical predictions of the hindered settling of polydisperse suspensions. The most popular is the MLB model (Lockett & Bassoon 1979; Masliyah 1979). The MLB model has been partially validated by comparison of predicted and experimentally measured concentration profiles following settling, starting at the initial time from a homogeneous suspension with a Gaussian particle size distribution (Xue & Sun 2003; Berres *et al.* 2005). This validation is not complete because the particle concentration at a given point in space is the sum of the concentrations of the different particle classes. Therefore, if a range of the particle size distribution makes a dominant contribution to the concentration, then an acceptably accurate prediction of the concentration profile may hide errors in the prediction of the velocity of certain particle classes. Furthermore, validation of the settling rates predicted by the MLB model for more than three size classes has not been published.

The MLB model reads

$$h_i(\boldsymbol{\phi}) = (1 - \phi)^{n-1} \left(1 - \sum_{j=1}^{m} \left(\frac{a_j}{a_i} \right)^2 \phi_j \right), \qquad (2.3)$$

where a_j/a_i is the ratio of the radii of the jth and the ith species. Appendix A contains details of the derivation of the MLB model, so that the model assumptions can be evaluated. The function $(1 - \sum_{j=1}^{m} (a_j/a_i)^2 \phi_j)$ is the hindered settling function obtained by including the effect of volume fraction on the fluid–solid slip velocity (a continuity effect), and neglecting the effect of hydrodynamic interactions on the drag force experienced by each particle. The prefactor $(1 - \phi)^{n-1}$ incorporates the effect of hydrodynamic interactions.

An even simpler model, which has been adopted by some authors (Davis & Hassen 1988; Abeynaike *et al.* 2012; Vowinckel *et al.* 2019; Chen *et al.* 2023), is based on the

model of Richardson & Zaki ([1954](#)) for monodisperse suspensions. It reads

$$h_i(\boldsymbol{\phi}) = (1 - \phi)^n, \tag{2.4}$$

where $n \approx 5$ (Brzinski & Durian [2018](#)). This model predicts different velocities for different particle radii a_i, because h_i contains the single-particle Stokes formula at denominator. In the current paper, this hindered settling formula is referred to as the Richardson–Zaki model for polydispersed suspensions.

3. Numerical approach and validation

Consider a polydisperse suspension of N spheres having the same density but different radii. The N spheres are divided into m size classes. The radius of size class i is a_i. Each sphere in class i is subjected to a force $\boldsymbol{F}_i = \frac{4}{3}\pi a_i^3 (\rho_p - \rho_f)\boldsymbol{g}$, which includes the particle weight and buoyancy; ρ_p and ρ_f are the densities of the spheres and the fluid, respectively, and $\boldsymbol{g}$ is the gravitational acceleration. The single-particle Stokes velocity corresponding to each class is $\boldsymbol{u}_{St,i} = 2/(9\mu)a_i^2(\rho_p - \rho_f)\boldsymbol{g}$, where μ is the dynamic viscosity of the fluid. In the current work, the particle velocity statistics are calculated from instantaneous random configuration of the spheres by first averaging over the particles in the computational domain and then ensemble-averaging over statistically identical configurations. Each configuration is generated by randomly placing the spheres one by one inside the computational domain, ensuring that each placement gives no overlap between the spheres (Revay & Higdon [1992](#); Wang & Brady [2015](#); Cheng & Wachs [2023a](#)) (we note that a simulation of settling under gravity of a random particle configuration is different from a simulation of uniform flow past fixed random arrays, because in the former case different particles have different velocities, while in the latter the relative velocity between the particles and the undisturbed fluid is uniform). An example of a random array configuration is shown in figure 1. In our coordinate system, gravity is aligned in the z direction, also referred to as the vertical direction in the following. The horizontal direction corresponds to the x and y coordinates.

To calculate the velocities of individual particles, a basic version of the Stokesian dynamics method is adopted (Brady *et al.* [1988](#); Brady & Bossis [1988](#)). While modern grid-based particle-resolved methods could be used (Willen & Prosperetti [2019](#); Yao, Criddle & Fringer [2021](#); Shajahan & Breugem [2023](#)), the Stokesian dynamics method is perfectly suitable for the objectives of the current paper: it is accurate in the relevant range of particle concentrations, it allows fast simulations and (unlike grid-based methods) it can simulate large ratios between the largest and smallest particle radii without numerical difficulties – a feature we would like to maintain for future highly polydisperse simulations. In the Stokesian dynamics method, the velocities of the spheres are calculated by solving the mobility problem

$$\boldsymbol{U} - \langle \boldsymbol{u} \rangle = \boldsymbol{M}\boldsymbol{F}, \tag{3.1}$$

where $\boldsymbol{U}$ is the $3N$ vector containing the velocities of the spheres, $\boldsymbol{F}$ is the $3N$ vector containing the gravitational forces acting on the spheres (these forces include the particle weight and the buoyancy force) and $\boldsymbol{M}$ is the $3N \times 3N$ mobility matrix (Kim & Karrila [2013](#)). In (3.1), $\langle \boldsymbol{u} \rangle$ is the average translational velocity of the suspension. In our simulations $\langle \boldsymbol{u} \rangle = \boldsymbol{0}$ because of the zero volume flux condition of batch sedimentation (Berres *et al.* [2005](#)). Note that in the current work only velocity–force coupling is considered, i.e. the stresslet and other force moments are not considered. Brady & Durlofsky ([1988](#)) showed that in a sedimenting suspension the inclusion of the stresslet
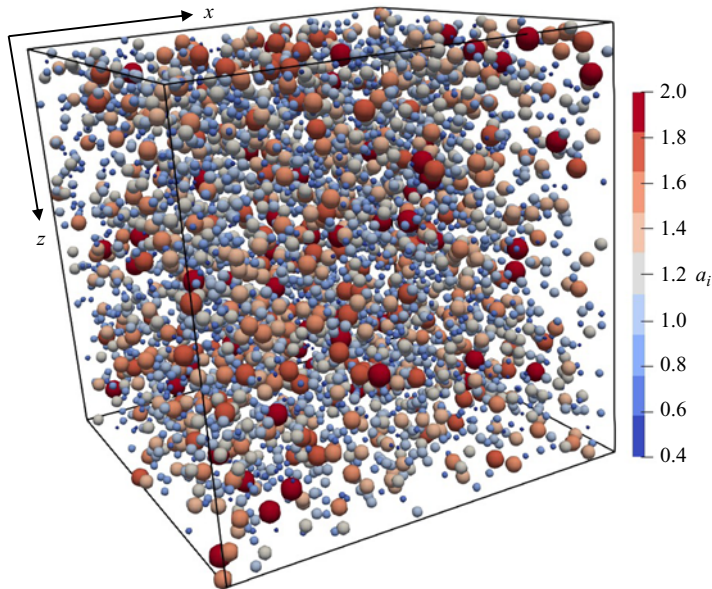
Figure 1. A configuration for volume fraction $\phi = 0.05$ and polydispersity parameter $\alpha = 0.4$. The spheres are coloured according to their radii.

changes the settling rate negligibly. Because we work in the relatively dilute limit, short-range lubrication forces are also neglected.

The mobility matrix $\boldsymbol{M}$ depends on the positions and radii of the spheres. We use the Rotne–Prager approximation for this term (Rotne & Prager 1969; Zuk *et al.* 2014). This approximation has been shown to give accurate predictions of the sedimentation velocities of suspensions from dilute to relatively dense (Brady & Durlofsky 1988). Triply periodic boundary conditions are applied to the simulation box. The mobility matrix is constructed using the Ewald summation technique by splitting the mobility matrix into a real-space part and a wave-space part (Beenakker 1986). Explicit formulae for the mobility matrix for a polydisperse suspension can be found in Beenakker (1986) and Hase & Powell (2001). As characteristic length and velocity scales, we choose the mean particle radius $\langle a \rangle$ and the single-particle Stokes velocity corresponding to $\langle a \rangle$. To make forces non-dimensional we use the effective weight of the mean particle, $\frac{4}{3}\pi\langle a \rangle^3 (\rho_p - \rho_f)g$.

In figure 2, numerical predictions for a single sphere in a triply periodic cubic box are plotted against Hasimoto's analytical solution (Hasimoto 1959) and the simulation results of Brady *et al.* (1988). The volume fraction of the simple cubic array is varied by varying the size of the box. Based on the point-force assumption, Hasimoto (1959) derived $u/u_{St} = 1 - 1.7601\phi^{1/3}$ for $\phi \ll 1$, where u_{St} is the Stokes velocity of the sphere. Brady *et al.* (1988) used Stokesian dynamics with different approximations for the mobility matrix. The results of Brady *et al.* (1988) shown in figure 2 correspond to simulations in the Rotne–Prager approximation. As seen from figure 2, our results match exactly those of Brady *et al.* (1988) and converge to Hasimoto's solution for $\phi \to 0$. This test validates our implementation of the Ewald summation for the periodic boundary conditions.

In figure 3, the normalised relative settling velocity is shown as a function of the normalised centre-to-centre distance between two unequal spheres with size ratios 2 and 5, respectively. In our simulations, the radius of the large sphere is fixed to $a_l = 2$. The radius of the small sphere is $a_s = 1$ and 0.4 for size ratios 2 and 5, respectively (these values are
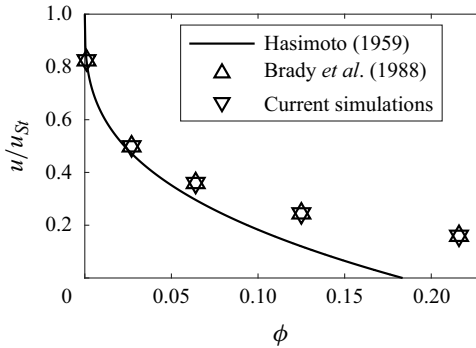
Figure 2. Normalised settling velocity versus volume fraction for a simple cubic array of monodisperse spheres. The line is the point-force solution of Hasimoto (1959). Upward triangles are the numerical results of Brady *et al.* (1988).
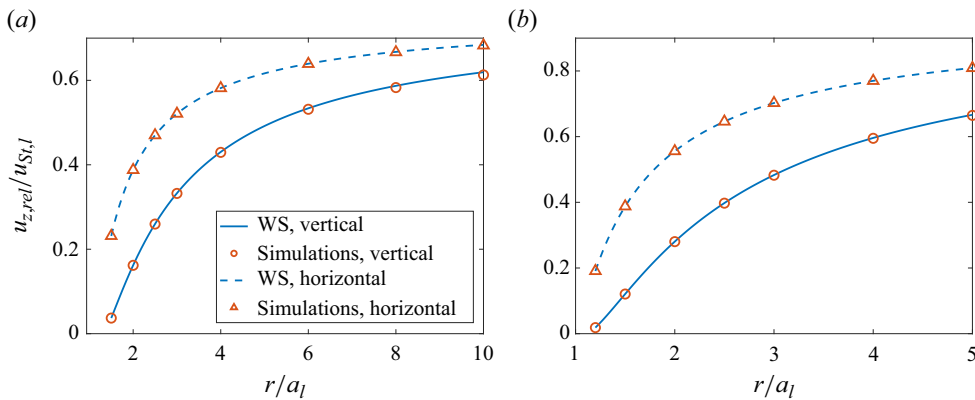

Figure 3. Normalised relative settling velocity for a pair of spheres as a function of the centre-to-centre distance for (*a*) size ratio 2 and (*b*) size ratio 5. Results of current simulations are shown as symbols and analytical results of Wacholder & Sather (1974) (WS) are shown as lines.

chosen because the largest radius is 2 and the largest size ratio is 5 in the polydisperse simulations analysed in this paper). The relative settling velocity between the two spheres is normalised by the Stokes velocity of the large sphere. The centre-to-centre distance is normalised by the radius of the large sphere. In figure 3, symbols are results from our simulations and lines correspond to the asymptotic solution of Wacholder & Sather (1974), in which only far-field hydrodynamic interactions were considered. It can be seen that our results match the analytical solution for both vertically and horizontally aligned pairs.

The current paper discusses results for bidisperse suspensions and polydisperse suspensions with more than two classes, also comparing with the monodisperse case. For the monodisperse case, the radius of the spheres is $a = 1$. For the bidisperse case, two size ratios are considered: $a_2/a_1 = 2$ and 5. The radii of the small size classes are $a_1 = 0.8$ and 0.4 for these two size ratios, respectively. The volume fraction of the small size class is $\phi_1 = \frac{3}{11}\phi$ for size ratio 2 and $\phi_1 = \frac{1}{76}\phi$ for size ratio 5. These volume fraction ratios are chosen so that the average radius of the spheres is equal to 1.0 for each system.

For the simulations with several size classes, the particle size distribution follows $p(a) = (1/a\sigma\sqrt{2\pi})\,e^{-(\ln a - \mu)^2/2\sigma^2}$, where the mean value of the size distribution is
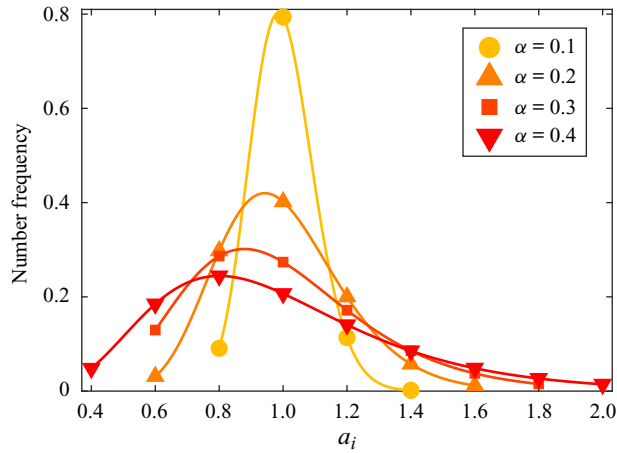
Figure 4. Discrete frequency distributions of particle size for different values of the polydispersity parameter (symbols). Lines indicate the continuous log-normal distributions that fit the discrete frequency histograms.
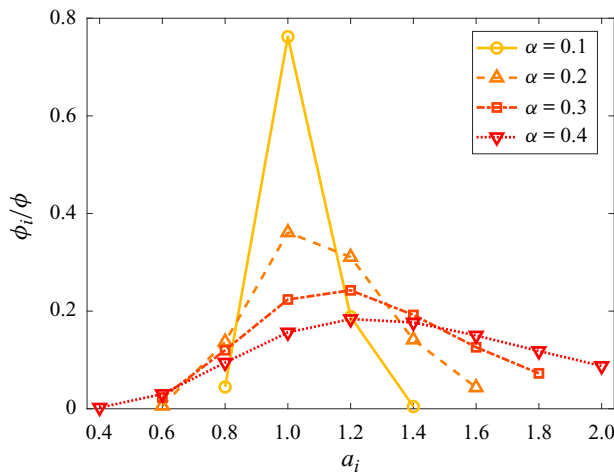

Figure 5. Volume fraction distributions for different values of α.

$\langle a \rangle = e^{\mu+\sigma^2/2}$ and the standard deviation is $\Delta a = \sqrt{(e^{\sigma^2}-1)\,e^{2\mu+\sigma^2}}$. We define the polydispersity parameter as $\alpha = \Delta a/\langle a \rangle$. Four size distributions are considered, with $\langle a \rangle = 1$ and $\alpha = 0.1$, 0.2, 0.3 or 0.4. Each distribution is cut at the two ends, resulting in a range $a_{min} \le a \le a_{max}$, where a_{min} and a_{max} are chosen so that at least 95 % of the original distribution falls within this range. The largest size ratio between two spheres is 5. Each radius range is discretized into between four and nine size classes, with a difference of 0.2 between the radii of two adjacent size classes.

The discrete number-frequency distributions are overlaid on the corresponding continuous distributions in figure 4. The frequency of size class i is calculated as $p(a_i)/\sum_{j=1}^{m} p(a_j)$. The corresponding volume-fraction distributions are shown in figure 5. For each value of α, the volume fraction ϕ ranges from 0.01 to 0.10. For each simulated case, corresponding to a combination of α and ϕ, a fixed box size $L = 80$ is used and 500 random particle configurations are generated. The total number of spheres in each case
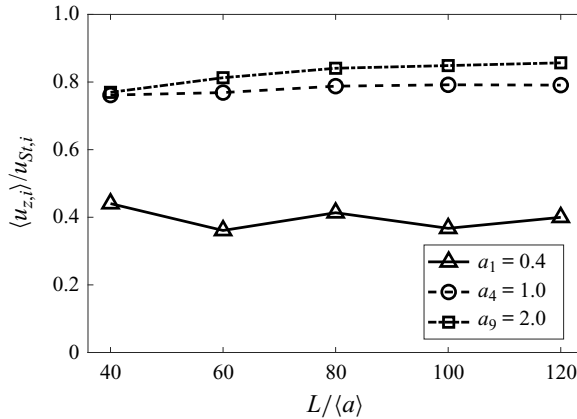
Figure 6. Normalised average settling velocity versus domain size for three selected size classes ($\phi = 0.03$ and $\alpha = 0.4$).

varies from 925 to 12 223. We have verified that increasing the size of the computational domain beyond $L = 80$ does not change the magnitude of the results significantly. As an example, in figure 6 we show the velocities of three size classes (for $\phi = 0.03$ and $\alpha = 0.4$) as a function of L.

The average velocity of class i is calculated by ensemble-averaging over M configurations as

$$\langle \bar{u}_{\xi,i} \rangle = \frac{\sum_{k=1}^{M} \bar{u}_{\xi,i}^{k}}{M}, \tag{3.2}$$

where $\xi = 1, 2, 3$ correspond to the three Cartesian coordinates, $\bar{u}_{\xi,i}$ is the intrinsic volume average of the velocity component $u_{\xi,i}$ within one configuration and $\langle \cdot \rangle$ is the ensemble-averaging operator. The intrinsic volume average within class i over configuration k is $\bar{u}_{\xi,i}^{k} = \sum_{l=1}^{N_i} u_{\xi,i,l}^{k}/N_i$, where N_i is the number of particles in class i. The standard deviation of a certain velocity component within one realisation is calculated as $(u_{\xi,i}')^k = \sqrt{\sum_{l=1}^{N_i}(u_{\xi,i,l}^k - \bar{u}_{\xi,i}^k)^2/(N_i - 1)}$. Averaging over many realisations gives an improved estimate of the class-averaged standard deviation. In the bulk of the paper we indicate averages by the bracket symbol, distinguishing between volume and ensemble average when necessary.

3.1. *Relation between the mobility formulation and Batchelor's formula*

In this section we show the connection between the mobility formulation, equation (3.1), and Batchelor's formula, equation (2.1). For simplicity of notation, let us consider a specific size class. Without loss of generality we consider class 1. According to (3.1) the velocity of the αth sphere in the first size class is

$$\boldsymbol{u}_{\alpha,1} = \sum_{i=1}^{m} \sum_{\beta=1}^{N_i} \boldsymbol{M}_{\alpha 1, \beta i} \boldsymbol{F}_i, \tag{3.3}$$

where N_i is the number of spheres in the ith class and $\boldsymbol{M}_{\alpha 1, \beta i}$ is the 3×3 mobility matrix representing the hydrodynamic interaction between the αth sphere in the first class and the

βth sphere in the ith class (Kim & Karrila 2013). Because $\boldsymbol{M}_{\alpha1,\alpha1} = (6\pi\mu a_1)^{-1}$, (3.3) can be written as

$$\boldsymbol{u}_{\alpha,1} = \boldsymbol{u}_{St,1} + \sum_{\beta \neq \alpha} \boldsymbol{M}_{\alpha1,\beta1}\boldsymbol{F}_1 + \sum_{i \neq 1} \sum_{\beta=1}^{N_i} \boldsymbol{M}_{\alpha1,\beta i}\boldsymbol{F}_i. \tag{3.4}$$

The average velocity of the first class in this configuration is

$$\bar{\boldsymbol{u}}_1 = \boldsymbol{u}_{St,1} + \frac{1}{N_1}\left(\sum_{\alpha}\sum_{\beta \neq \alpha} \boldsymbol{M}_{\alpha1,\beta1}\boldsymbol{F}_1 + \sum_{\alpha}\sum_{i \neq 1}\sum_{\beta=1}^{N_i} \boldsymbol{M}_{\alpha1,\beta i}\boldsymbol{F}_i\right), \tag{3.5}$$

but because $\boldsymbol{F}_i$ is constant within the same size class, we can also write

$$\bar{\boldsymbol{u}}_1 = \boldsymbol{u}_{St,1} + \boldsymbol{s}_{11}\boldsymbol{F}_1 + \sum_{i \neq 1} \boldsymbol{s}_{1i}\boldsymbol{F}_i, \tag{3.6}$$

where $\boldsymbol{s}_{11}$ and $\boldsymbol{s}_{1i}$ describe the intra-class hydrodynamic interactions (within the first class) and the inter-class hydrodynamic interactions (between the first and the ith classes), respectively. These two matrices can be written as $\boldsymbol{s}_{11} = (N_1 - 1)\bar{\boldsymbol{M}}_{11}$ and $\boldsymbol{s}_{1i} = N_i\bar{\boldsymbol{M}}_{1i}$, where $\bar{\boldsymbol{M}}_{11}$ and $\bar{\boldsymbol{M}}_{1i}$ are the average two-sphere mobility matrices. Upon ensemble-averaging, the average velocity of the first size class can be written as

$$\langle\bar{\boldsymbol{u}}_1\rangle = \boldsymbol{u}_{St,1} + \langle\boldsymbol{s}_{11}\rangle\boldsymbol{F}_1 + \sum_{i \neq 1}\langle\boldsymbol{s}_{1i}\rangle\boldsymbol{F}_i. \tag{3.7}$$

The average velocity component in the gravity direction can be written as

$$\frac{\langle u_1\rangle}{u_{St,1}} = 1 + \frac{9\mu\langle s_{11}\rangle}{2a_1^2 n_1}\phi_1 + \sum_{i \neq 1}\frac{9\mu\langle s_{1i}\rangle}{2a_1^2 n_i}\phi_i, \tag{3.8}$$

where the formula for the single-particle Stokes velocity is used and n_i is the number density of class i. The scalar $\langle s_{1i}\rangle$ is the component of $\langle\boldsymbol{s}_{1i}\rangle$ for the velocity–force coupling in the gravity direction.

Extending (3.8) to a generic class i yields

$$\frac{\langle u_i\rangle}{u_{St,i}} = 1 + B_{ii}(\boldsymbol{\phi})\phi_i + \sum_{j \neq i} B_{ij}\left(\boldsymbol{\phi}, \frac{a_j}{a_i}\right)\phi_j. \tag{3.9}$$

The dependence of B_{ii} and B_{ij} on the volume fraction vector $\boldsymbol{\phi}$ comes from the fact that $\langle s_{ij}\rangle$ depends on the pair distribution functions, and the pair distribution functions in turn depend on the volume fraction of each class. The dependence of B_{ij} on a_j/a_i comes from the dependence of the two-sphere mobility matrix on the size ratio. For $\phi \to 0$, B_{ii} is a constant and $B_{ij} = S_{ij}$ is only a function of a_j/a_i. In this limit, (3.9) recovers Batchelor's expression (2.1).

4. Hindered settling of monodisperse and bidisperse suspensions

To build confidence in the ability of the numerical method to predict settling data in more complex situations, we compare our simulations against settling models for monodisperse and bidisperse suspensions. For the monodisperse case, the comparison also provides a
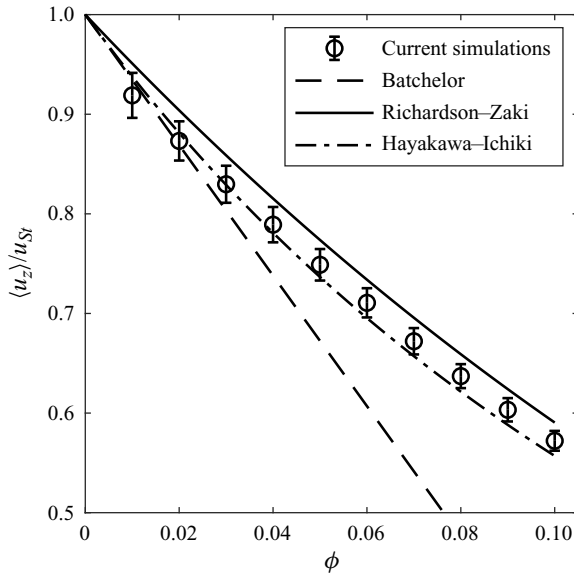
Figure 7. Monodispese case: average settling velocity, normalised by the single-particle Stokes velocity, versus volume fraction.

validation of our numerical approach. Indeed, the empirical or semi-analytical models are well established in their regime of validity: the Richardson–Zaki correlation summarises experimental data obtained by those authors, and its validity has been confirmed in numerical simulations (Cunha *et al.* 2002; Abbas *et al.* 2006) and independent experiments (Nicolai *et al.* 1995); the analytical model of Batchelor for monodispersed suspensions is exact for $\phi \ll 1$ (Davis & Acrivos 1985); and the Hayakawa–Ichiki model has been favourably compared against monodisperse simulations for a wide range of volume fractions (Padding & Louis 2004).

The normalised average settling velocity $\langle u_z \rangle / u_{St}$ for the monodisperse suspension is plotted in figure 7 as a function of ϕ. We include in the plot the Richardson–Zaki correlation $(1 - \phi)^n$ (Richardson & Zaki 1954) for $n = 5$, the Batchelor model $1 + S\phi$ (Batchelor 1972) assuming $S = -6.55$ and the Hayakawa–Ichiki model $(1 - \phi)^3 / (1 + 2\phi + 1.429\phi(1 - \phi)^3)$ (Hayakawa & Ichiki 1995). The values chosen for the exponent n and the coefficient S here are typically for non-Brownian particles interacting only hydrodynamically (Padding & Louis 2004; Moncho-Jordá, Louis & Padding 2010).

Our simulation results agree with Batchelor's model for ϕ approximately smaller than 0.03. For larger volume fractions, the simulation gives larger values than Batchelor's model. A similar range of validity for Batchelor's model was also found by Abbas *et al.* (2006) using a force-coupling method. Our results also agree well with the Hayakawa–Ichiki model for $\phi \leq 0.05$ and they lie between the predictions of the Richardson–Zaki correlation and the Hayakawa–Ichiki model for $\phi \geq 0.06$. The simulation data for $\phi = 0.01$ are smaller than the values predicted by the three models. This is expected because of the use of triply periodic boundary conditions in a domain of finite size (Phillips, Brady & Bossis 1988).

Normalised average settling velocities for the small and the large particles in the bidisperse case are plotted as symbols in figure 8 for two size ratios. The predictions of Batchelor's model (2.1), Davis & Gecol's model (2.2) and the MLB model (2.3) are
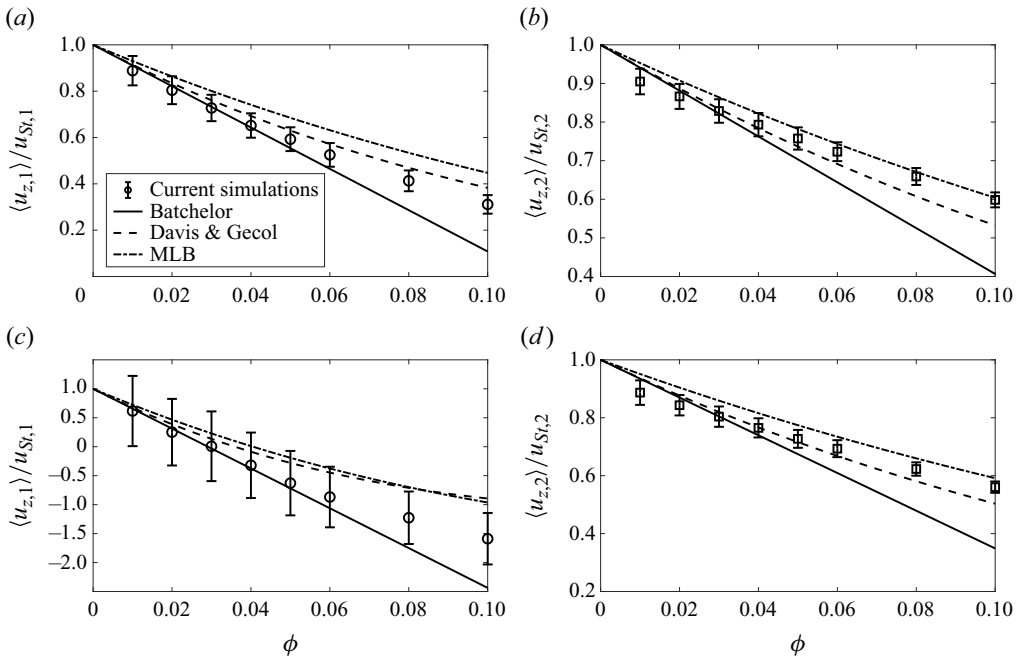
Figure 8. Bidisperse case: average settling velocity normalised by the single-particle Stokes velocities for the small (*a*,*c*) and large (*b*,*d*) particles. (*a*,*b*) Size ratio 2. (*c*,*d*) Size ratio 5.

indicated by lines. It is seen from figure 8(*a*,*c*) that our results for the small particles agree with the predictions of Batchelor's model for $\phi \leq 0.05$, and lie between the predictions from Batchelor's model and Davis & Gecol's model for $\phi \geq 0.06$. For the large particles, our results agree with predictions from Batchelor's model for $\phi \leq 0.03$ and lie between the predictions from the Davis & Gecol and MLB models for $\phi \geq 0.04$. Stokesian dynamics calculations by Wang & Brady (2015) that include stresslet and lubrication contributions also predicted for ϕ larger than around 0.05 hindered settling velocities smaller and larger than those of the Davis & Gecol model for the small and the large particles, respectively. Our results of the bidisperse case are therefore in line in terms of trends with those of Wang & Brady (2015).

5. Polydisperse suspensions

5.1. *Velocity statistics*

Before delving into the analysis of the mean settling velocity, we analyse the probability distribution of particle velocities in the polydisperse particle simulations. This information enables a characterisation of the statistical representativeness of the mean values. To illustrate the spatial distribution of particle velocities, in figure 9 we show snapshots of the simulations with each sphere coloured according to its settling velocity. Spheres coloured in red have settling velocities in the direction of gravity whereas spheres coloured in blue have settling velocities opposite to gravity. Figure 9(*c*) shows that the smaller particles can move against gravity, and have negative velocities comparable in magnitude to the positive settling velocity of the largest particles.

Probability distribution functions (PDFs) of horizontal and vertical velocities, shown in figure 10 for different values of α, are approximately Gaussian, with a variance that increases as α increases. These PDFs are constructed by considering all the particles
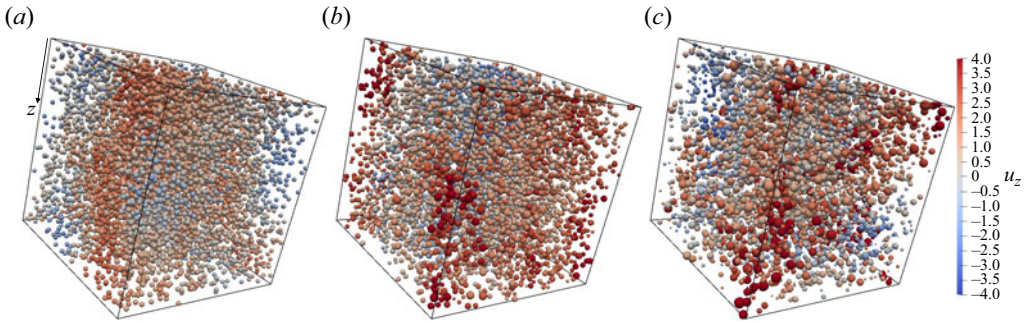
Figure 9. Configuration for different polydispersity parameters and $\phi = 0.05$, with the spheres coloured according to their settling velocity, for (a) $\alpha = 0$, (b) $\alpha = 0.2$ and (c) $\alpha = 0.4$.
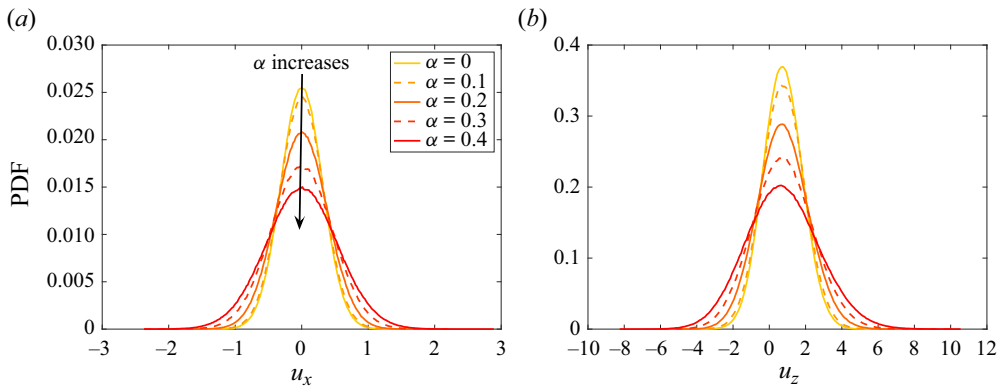

Figure 10. The PDFs of (a) horizontal and (b) vertical velocities for different polydispersity parameters and $\phi = 0.05$.
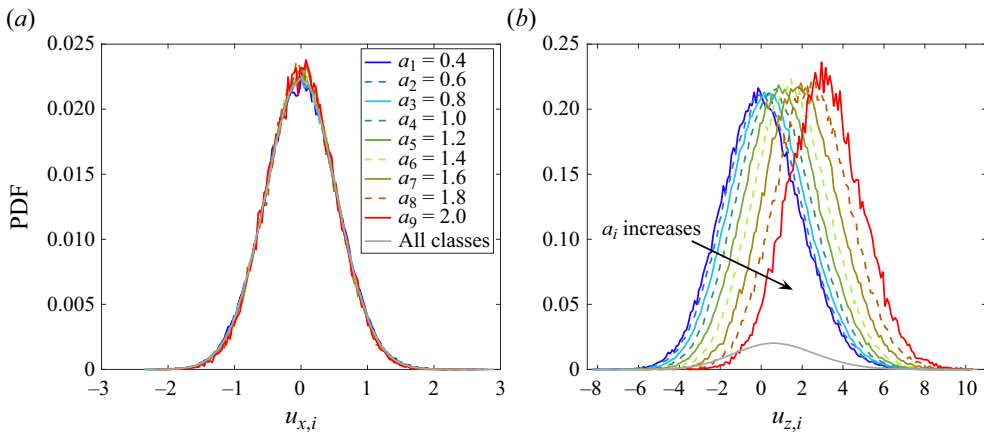

Figure 11. The PDFs of (a) horizontal and (b) vertical velocities for $\alpha = 0.4$ at $\phi = 0.05$. In contrast to figure 10, here the PDFs are calculated based on the distribution of velocities within each size class.

in the simulation domain. However, spheres belonging to the same size class also have a distribution of settling velocities. Therefore, in figure 11, we show the PDFs of the horizontal and the vertical velocities of spheres in each size class for $\alpha = 0.4$. For comparison, the PDFs of the velocities of all the spheres are included in this plot as
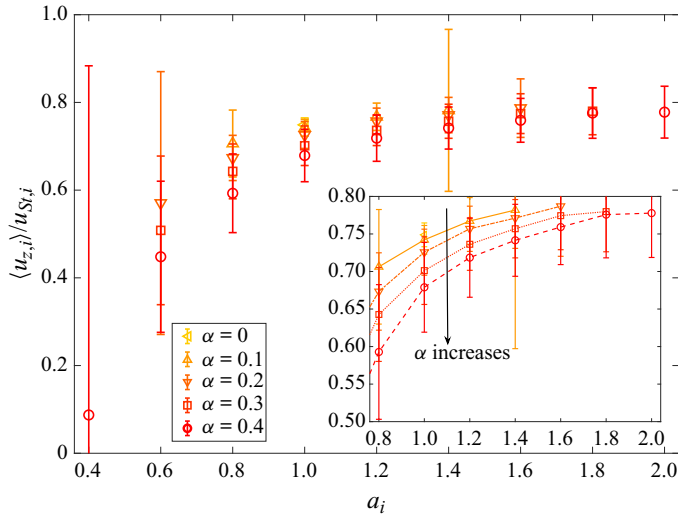
Figure 12. Normalised average settling velocity of each size class for different polydispersity parameters and $\phi = 0.05$. The inset is a zoom in the range $0.8 \leq a_i \leq 2$. The lines are guides for the eye.

grey lines. Again, the PDFs are approximately Gaussian (simulations by Cheng & Wachs (2023*a*) of uniform flow past fixed polydisperse random arrays indicate also a Gaussian distribution for the hydrodynamic forces of a given size class). Surprisingly, the PDFs of the horizontal velocities for different size classes collapse onto a single curve (figure 11*a*). From the PDFs of the vertical velocities in figure 11(*b*), it is seen that the mean velocity increases as the size of the particles increases, and different size classes have comparable variances.

The average vertical settling velocity of each size class normalised by the corresponding single-particle Stokes velocity is shown in figure 12 for different values of α. The inset shows a zoom in the range $0.8 \leq a_i \leq 2$. Because now the settling velocity is normalised by the single-particle settling velocity, the information in this plot complements the data of figure 11(*b*). We see that for fixed α the normalised average settling velocity increases as the particle size increases. This means that the velocities of small particles are more hindered than the velocities of large particles. For a given size class, the normalised average settling velocity decreases as α increases, and decreases faster for small particles than for large particles. The standard deviation around the mean seems to decrease with a_i, except for values near $a_i = 1.4$ (we have examined the velocity probability distributions of several configurations and found no probability distributions with atypical behaviour of the $a_i = 1.4$ class; no simple explanation was found for this anomalous data point).

In the previous figures, the total volume fraction was fixed, and α was changed. In figure 13, we instead change ϕ for fixed $\alpha = 0.4$. This plot confirms the trend seen in figure 12: for a given volume fraction, the normalised average settling velocity decreases as the particle size decreases. The normalised average settling velocity decreases faster with increasing ϕ for small-size particles.

To summarise, the smaller particles are more hindered and more affected by polydispersity than the large ones.

Statistical deviations with respect to the mean particle velocity, as measured by the root mean square of the velocity fluctuation, increase as α or ϕ increase (see figures 14 and 15). The normalised horizontal and vertical velocity fluctuations of each size class are
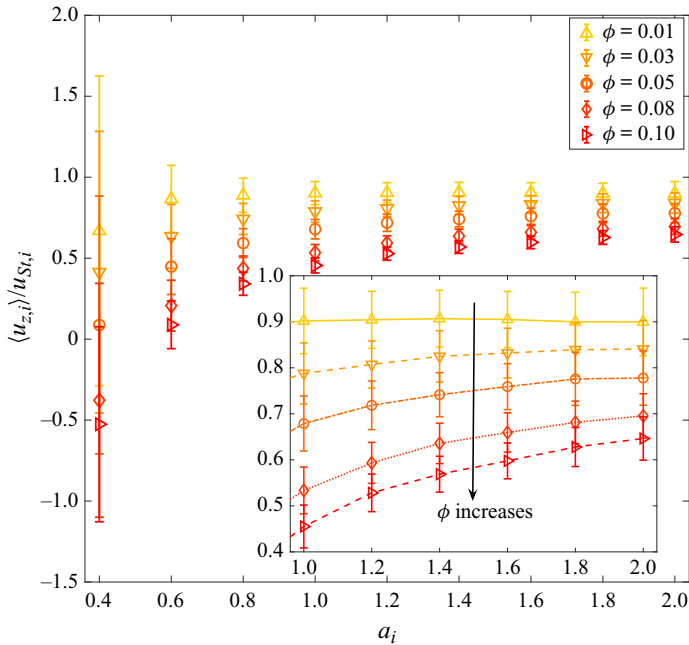
Figure 13. Normalised average settling velocities of each size class, for $\alpha = 0.4$ and different volume fractions. The inset shows a zoom in the range $1 \leq a_i \leq 2$.
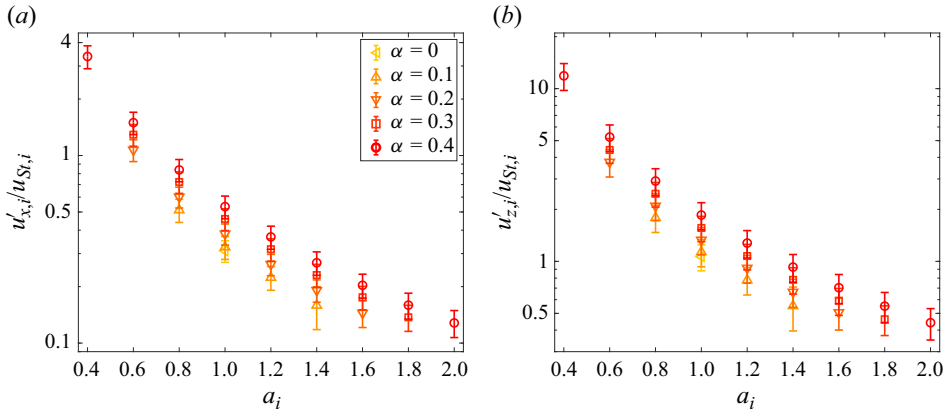

Figure 14. Normalised (*a*) horizontal and (*b*) vertical velocity fluctuations for different α and $\phi = 0.05$.

shown for $\alpha = 0.2$ and 0.4 with fixed $\phi = 0.05$ in figure 16. For a fixed α, the normalised velocity fluctuations decrease as the particle size increases. Figure 11 seems to suggest that the velocity fluctuations are approximately independent of the particle radius a_i. Because the Stokes velocity scales as a_i^2, it is expected that the velocity fluctuations normalised by the Stokes velocity scale as $\sim a_i^{-2}$. Our data confirm this scaling (see lines in figure 16): $u_i'/u_{St,i} = c a_i^{-2}$ fits the data for all the values of α and ϕ simulated, as shown in tables 1 and 2. This scaling is also observed in our simulations of bidisperse suspensions: the ratio of velocity fluctuations between the two classes in these simulations is close to 1. Peysson & Guazzelli (1999) measured experimentally the velocity fluctuations of small and large
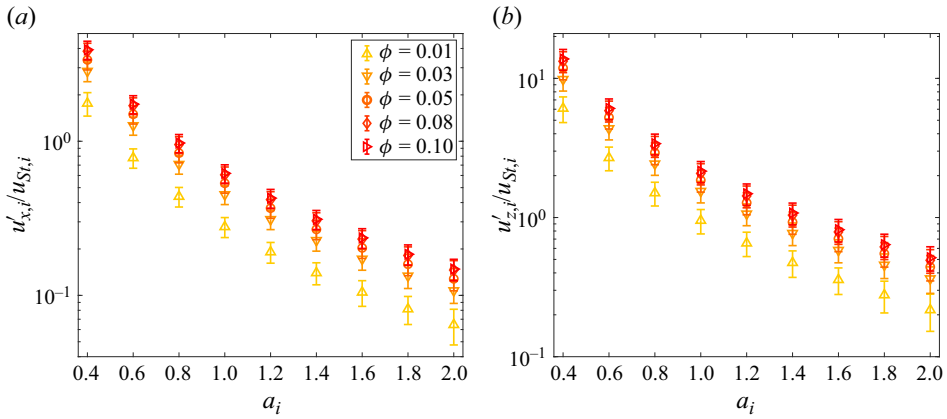
(*a*)

(*b*)

Figure 15. Normalised (*a*) horizontal and (*b*) vertical velocity fluctuations for different ϕ and $\alpha = 0.4$.
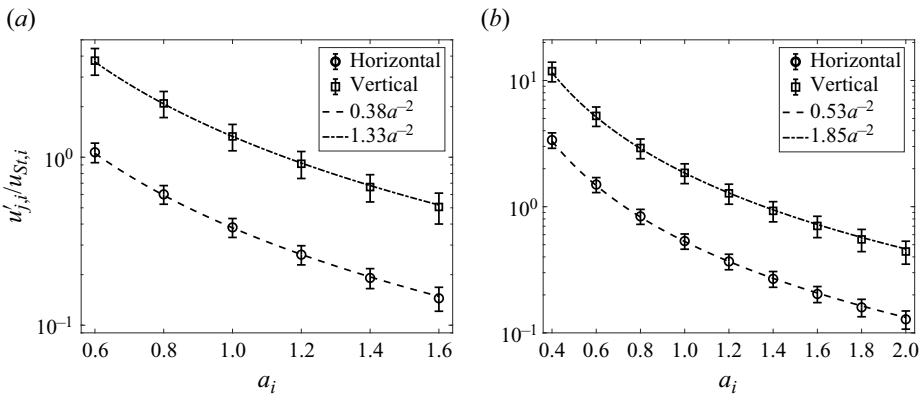
(*a*)

(*b*)

Figure 16. Normalised velocity fluctuations of each size class at $\phi = 0.05$ for (*a*) $\alpha = 0.2$ and (*b*) $\alpha = 0.4$.

α	Horizontal direction	Vertical direction
0.1	0.32	1.13
0.2	0.38	1.33
0.3	0.46	1.56
0.4	0.53	1.85

Table 1. Approximate values of the prefactor c in the scalings of the horizontal and the vertical normalised velocity fluctuations for each α at $\phi = 0.05$.

particles in a dilute bidisperse suspension with size ratio 2. They found that the ratios of velocity fluctuations between the small and the large size classes were around 0.85 and 0.75 in the vertical and horizontal directions, respectively, yielding a ratio roughly close to ours.

The anisotropy ratio between the vertical and the horizontal velocity fluctuations, plotted in figure 17, is around 3.5 regardless of the values of α or ϕ. This value was also observed in the monodisperse and bidisperse simulations.

1001 A30-16

ϕ	Horizontal direction	Vertical direction
0.01	0.28	0.95
0.03	0.45	1.54
0.05	0.53	1.85
0.08	0.61	2.08
0.10	0.62	2.15

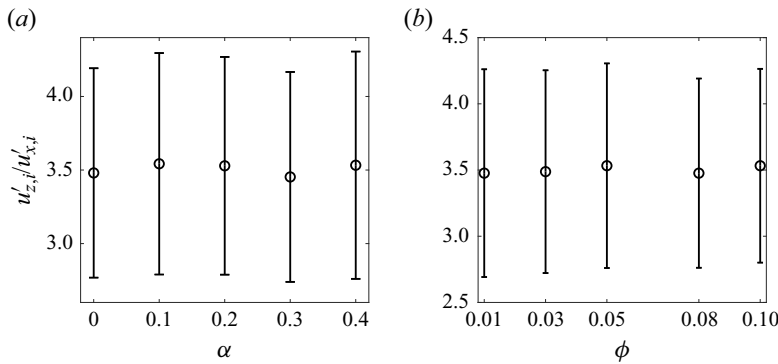Table 2. Same as table 1 but for different ϕ at $\alpha = 0.4$.

Figure 17. Ratio between vertical and horizontal velocity fluctuation magnitudes for $a_i = 1$ and (*a*) different α at $\phi = 0.05$ and (*b*) different ϕ at $\alpha = 0.4$.

5.2. *Comparison with hindered settling models*

In this subsection, current simulations are compared with predictions from Batchelor's (see (2.1)), Davis & Gecol's (see (2.2)) and the MLB (see (2.3)) models. The accuracy of the Richardson–Zaki correlation (see (2.4)) for polydisperse suspensions is also checked. The values of the coefficients S_{ij} in Batchelor's and Davis & Gecol's models are calculated from $S_{ij} = -3.50 - 1.10\lambda - 1.02\lambda^2 - 0.002\lambda^3$, where $\lambda = a_j/a_i$ (Davis & Gecol 1994). The value of the exponent n in the MLB model and the Richardson–Zaki correlation is 5.

Hindered settling functions corresponding to different size classes for fixed $\phi = 0.05$ and different α are compared against different theoretical models in figure 18. The Richardson–Zaki correlation largely overestimates the hindered settling functions of smaller particles, whereas it gives reasonable values for larger particles. The discrepancy between the Richardson–Zaki correlation and the computed hindered settling functions of smaller particles increases as α increases. For each α, the predictions from the other three models show a consistent trend for each size class. The MLB model gives the largest settling velocities, Batchelor's model gives the smallest settling velocities and Davis & Gecol's model gives intermediate values. The differences between the predictions from these three models get smaller as the particle size increases.

Figure 19 shows the normalised relative differences between the computed and predicted average settling velocities. The Batchelor model and the Davis & Gecol model predict the average settling velocity of each size class quite well for all α considered here, with relative errors smaller than 10 %, except for the smallest size class $a_i = 0.4$ for $\alpha = 0.4$ for which the simulation gives a very small settling velocity. From figure 19(*c*), it is seen that the relative difference between the predictions from the MLB model and the current
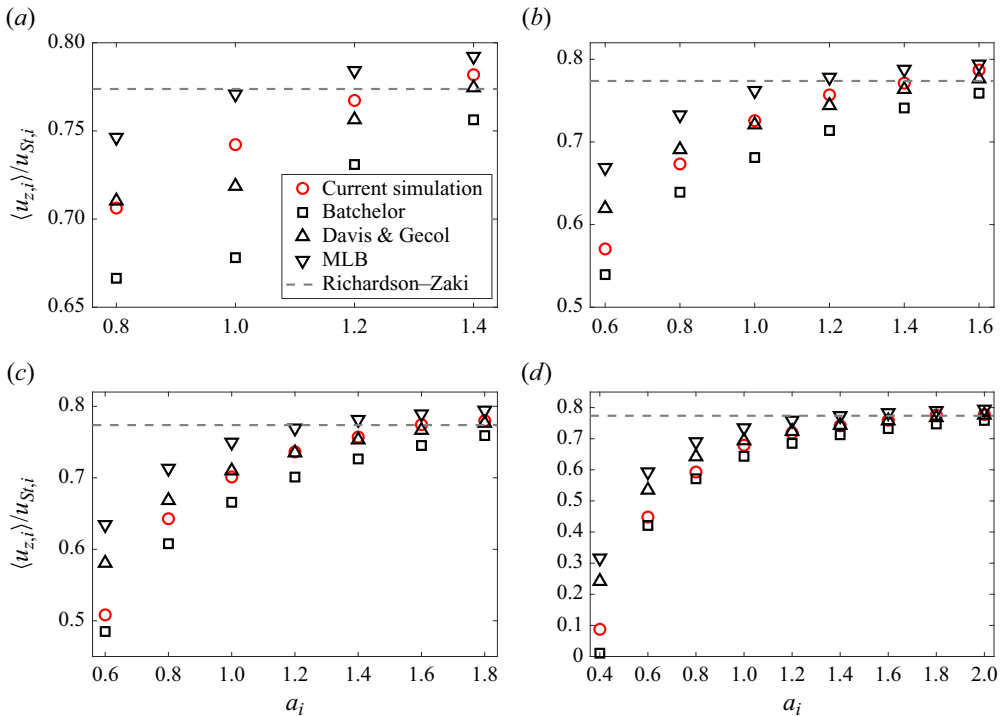
Figure 18. Comparison between the current simulation results and the predictions of hindered settling function models for the average velocity of different size classes, for $\phi = 0.05$ and different polydispersity parameters: (a) $\alpha = 0.1$, (b) $\alpha = 0.2$, (c) $\alpha = 0.3$ and (d) $\alpha = 0.4$.

simulations decreases as a_i increases, or α decreases. For $a_i \geq 1$, the MLB model predicts the average settling velocities quite well, with the relative difference within 10 %. For $a_i \leq 0.8$, the MLB model starts failing.

Hindered settling function data for fixed $\alpha = 0.4$ and different ϕ are compared with the predictions from different models in figure 20. Also, the Richardson–Zaki correlation predicts the hindered settling functions of smaller particles poorly. For the other three models, a trend in the predicted values is observed similar to that in the case of varying α. The predictions from the MLB model and the Davis & Gecol model are quite close to each other for all size classes at each volume fraction, and they are also quite close to the values from current simulations for larger particles. However, the Davis & Gecol model slightly underestimates the hindered settling functions of the larger particles when $\phi > 0.06$. For smaller particles, the predictions from the MLB model and the Davis & Gecol model are larger than the values from the simulations, and the discrepancies between the predictions from these two models and the values from current simulations get larger as ϕ increases. The predictions of Batchelor's model are close to the simulated values for ϕ approximately less than 0.05. As ϕ increases, Batchelor's model underestimates the hindered settling functions of all size classes systematically compared with the results of current simulations.

For fixed $\alpha = 0.4$, the relative differences between the average settling velocities predicted by different models and calculated by current simulations of each size class for different volume fractions are shown in figure 21. For each size class, the relative difference between the prediction from the Batchelor model and the current simulations increases as
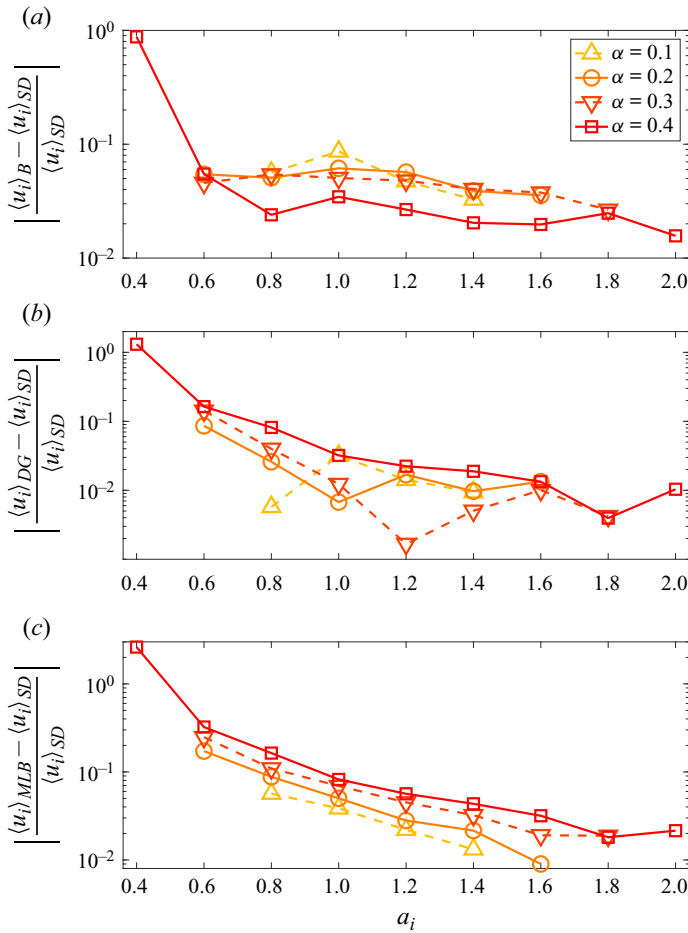
Figure 19. Relative differences between the average settling velocities from different models and from the current simulations for fixed $\phi = 0.05$: (*a*) the Batchelor model; (*b*) the Davis & Gecol model; (*c*) the MLB model.

the volume fraction increases, and it is within 10 % when $\phi \leq 0.05$, except for the smallest size class $a_i = 0.4$. From figure 21(*b*,*c*), it is seen that the relative differences are quite close for the Davis & Gecol and the MLB models, with those of the MLB model slightly larger. For larger size classes ($a_i \geq 1$), both these models give quite accurate predictions for all volume fractions considered, with the relative differences within 10 % compared with the results of current simulations. For smaller size classes ($a_i \leq 0.8$), both these models give predictions with large relative differences compared with the results of current simulations, and in general the relative difference gets larger as volume fraction increases or as size of the class decreases.

5.3. *Velocity slip*

We saw that the MLB model, despite its simplicity, gives relatively good agreement for large particles. However, it fails for small particles. The MLB model is based on a closure relation for the particle–fluid velocity difference (see Appendix A).
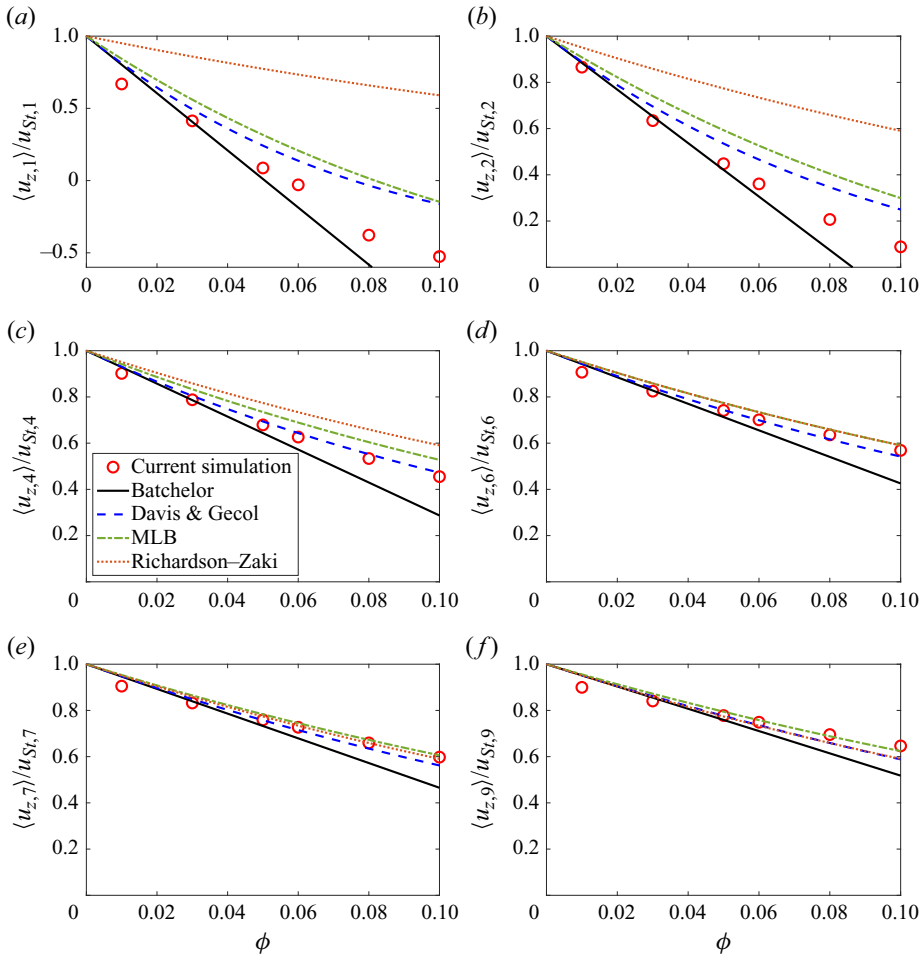
Figure 20. Comparison between the current numerical results and the predictions of different models. The comparison is here evaluated as a function of ϕ for fixed $\alpha = 0.4$. (*a–f*) Size classes a_1, a_2, a_4, a_6, a_7 and a_9, respectively.

Therefore, to understand the limits of validity of the model, we compute the slip velocity from the simulation data and compare against the MLB model prediction.

Slip velocities for each size class normalised by the corresponding Stokes velocities are plotted in figure 22 for $\phi = 0.05$ and different α. The slip velocity for size class i is defined as the difference between the average settling velocity of class i and the average velocity of the fluid phase:

$$u_{slip,i} = \langle u_{z,i} \rangle - \langle u_f \rangle. \tag{5.1}$$

The value of $\langle u_f \rangle$ is obtained from the zero-volume-flux condition $\sum \phi_j \langle u_{z,j} \rangle + (1 - \phi)\langle u_f \rangle = 0$. The slip velocity predicted by the MLB model is calculated from (see Appendix A)

$$u_{slip,i} = u_{St,i}(1 - \phi)^{n-1}. \tag{5.2}$$

It is seen that the MLB model does not predict accurately the slip velocities of the smaller particles. The discrepancy between the MLB model prediction and the simulation data increases as α increases. The slip velocities of relatively large particles are reasonably

1001 A30-20
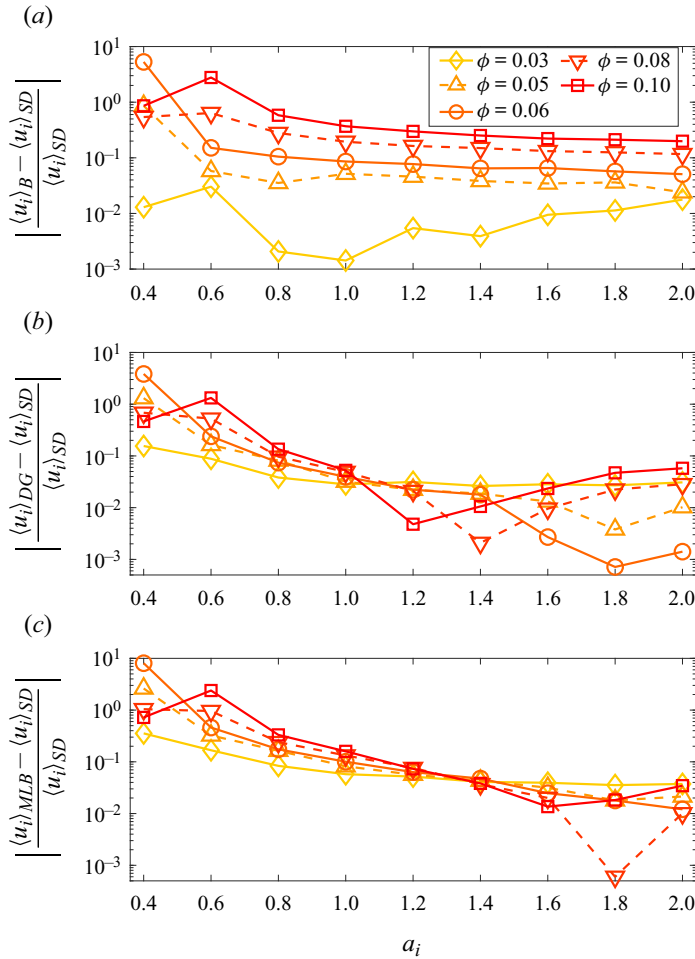
(*a*)

(*b*)

(*c*)

Figure 21. Same as in figure 19, but for different volume fractions and fixed $\alpha = 0.4$.

well captured. As the particle size increases, the simulation data tend to converge to the MLB model prediction.

The normalised slip velocities for each size class for fixed $\alpha = 0.4$ and varying ϕ are plotted in figure 23. It is seen that the prediction of the MLB model gets increasingly worse as the volume fraction increases for the small size classes. Predictions for the largest particles are instead acceptable regardless of the volume fraction.

6. Comparison with dynamic simulations

In our simulations, we ensemble-average over random particle configurations. This approach has been used by several authors, leading to quantitative predictions such as the average sedimentation velocities and velocity fluctuations of particles in monodisperse and bidisperse suspensions (Revay & Higdon 1992; Cunha *et al.* 2002; Abbas *et al.* 2006; Wang & Brady 2015). Phenomena of particle clustering or segregation could in principle be important in our simulations. Regarding segregation, Batchelor & Janse Van Rensburg (1986) have proven that in settling polydisperse suspensions of spheres having the same
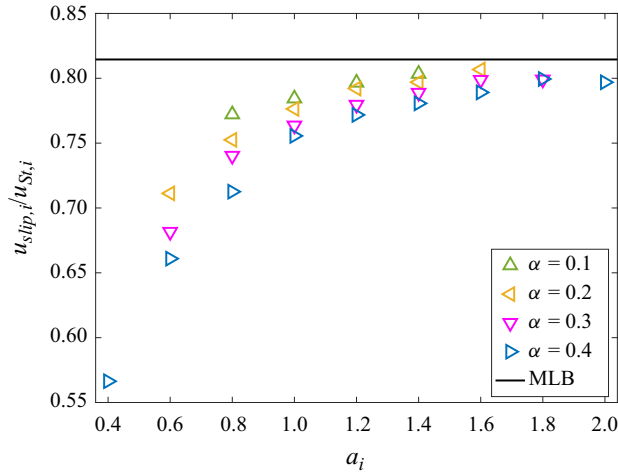
Figure 22. Normalised slip velocity for each size class for $\phi = 0.05$ and different α. The line shows the prediction of the MLB model.
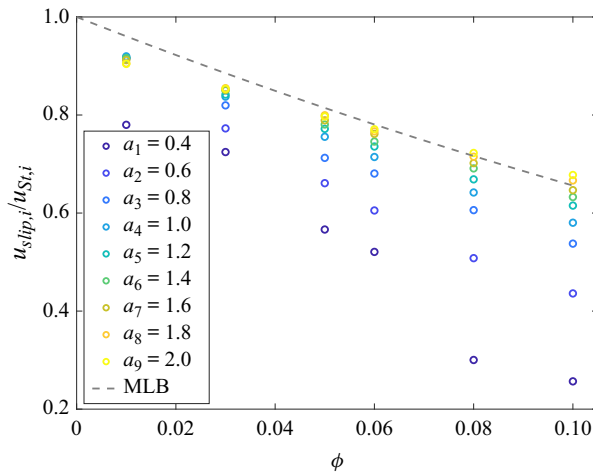

Figure 23. Normalised slip velocity for each size class for $\alpha = 0.4$ and different values of ϕ. The dashed line is the prediction of the MLB model.

density but different radii, particle class segregation (i.e. the tendency of particles of the same class to accumulate in specific locations) in general does not occur (the polydisperse suspension is practically homogeneous). Furthermore, in our range of parameters the suspension is dilute and phenomena of particle clustering (regardless of the class to which the particles belong) are expected not to be dominant features.

To assess the validity of our simulation approach, we have carried out selected dynamic simulations. For these simulations, we chose a domain size $L = 56$, a volume fraction of 0.05 and $\alpha = 0.4$. Initially the particles are randomly distributed. In the dynamic simulations, at each time step the particle velocities are calculated from (3.1) and the particle positions are updated by a two-step, explicit method. The settling velocity of the suspension is shown as a function of time in figure 24.
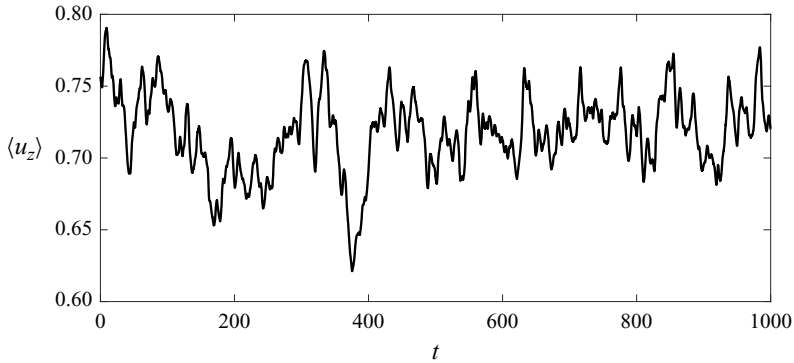
1001 A30-22

Figure 24. Dynamic simulation: settling velocity of the suspension, averaged over all the particles, as a function of time.
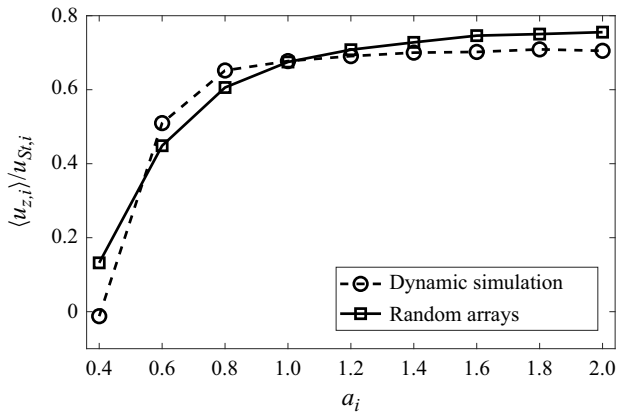

Figure 25. Normalised average settling velocity of each size class comparing the dynamic and the 'random array' simulations.

The normalised average settling velocities of each size class from dynamic simulations and random arrays are plotted in figure 25 (instantaneous results from dynamic simulations are time-averaged over $500 \leq t \leq 1000$). Differences between the hindered setting functions in the dynamic simulation and random arrays are visible. The particle velocity is seen to be slightly smaller in dynamic simulations than that in the random array simulations, except for the two size classes $a_i = 0.6$ and $a_i = 0.8$ where the reverse is true. However, the differences are comparatively small and the trends of the dynamic and static simulations are identical. The PDFs of the horizontal velocities of spheres in each size class from the dynamic simulation are shown in figure 26. Most of the PDFs collapse onto each other, as in the random array case, except the PDFs of larger size classes which show some relatively minor deviations. In figure 27, the pair distribution functions between the smallest and the largest size classes are plotted for both dynamic simulations and the random array simulations. Despite the statistical noise (which is more severe in polydisperse simulations than in monodisperse simulations due to the smaller number of particles per size class), the two pair distributions appear quantitatively similar. Strong clustering in the dynamic simulations would lead to pair distribution function values significantly larger than 1 for close interparticle distances. Instead, the values of the pair distribution functions at close separations are similar in range to those of the
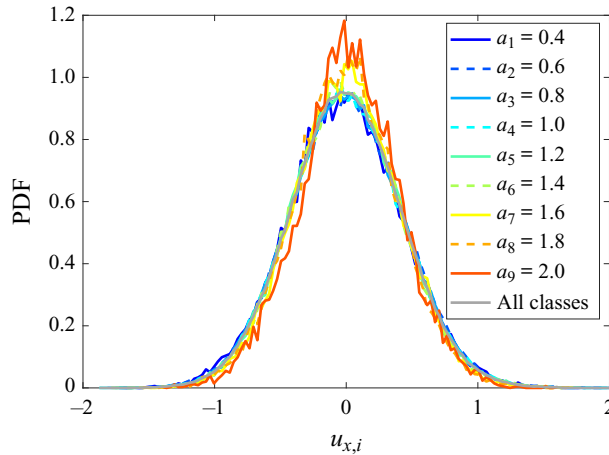
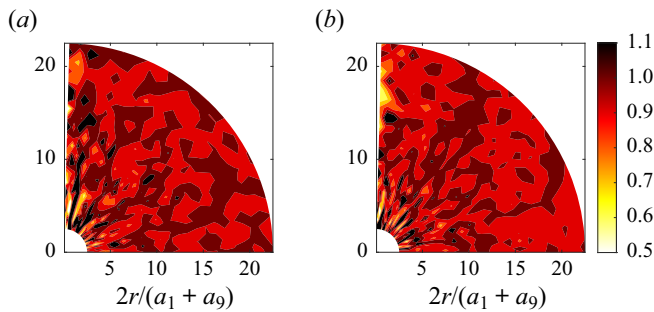Figure 26. The PDFs of horizontal velocities of spheres in each size class from the dynamic simulations.

Figure 27. Pair distribution functions of particle positions (between the smallest and the largest size classes) for (*a*) 'random array' and (*b*) dynamic simulations.

static simulations, and do not exceed 1.05. The results of the current section suggest that in our range of parameters phenomena of clustering, if present, are not sufficiently strong to affect the results presented in the current paper. A movie of the dynamic simulation for $\phi = 0.05$ and $\alpha = 0.4$ is provided as a supplementary movie available at https://doi.org/10.1017/jfm.2024.1068. This visualisation further confirms that no evident clustering effects are seen in our range of parameters.

7. Summary and discussion

The hindered settling function for non-Brownian, inertialess, dilute suspensions of polydisperse spheres with a log-normal size distribution was quantified via Stokesian dynamics simulations, considering the effects of the polydispersity parameter α and the volume fraction ϕ. This is the first paper that reports the velocity of each particle class for a log-normally distributed system with number of classes larger than three. The class-averaged settling velocity $\langle u_{z,i} \rangle$ of each particle size class was found to decrease for increasing α. The strongest dependence on the parameters was found in the range of small particles: $\langle u_{z,i} \rangle$ decays, with increasing ϕ or increasing α, faster for the smaller particles than for the largest particles, indicating a larger effect of hydrodynamic interactions on the lower tail of the particle size distribution.

1001 A30-24

The probability distribution functions of horizontal and vertical velocities of each size class tend to follow approximately a Gaussian distribution. The magnitude of the horizontal and vertical velocity fluctuations for each size class increases as ϕ or α increases, and appears to follow the approximate scaling $u'_i \sim u_{St,i}(a_i/\langle a \rangle)^{-2}$. Our simulations for the log-normally dispersed system suggest a value of about 3.5 for the anisotropy ratio between the vertical and the horizontal velocity fluctuations. This value is comparable to that observed in our simulations for monodisperse or bidisperse suspensions.

A detailed comparison with available theoretical models has been proposed. The accuracy of the Richardson–Zaki correlation for polydispersed suspensions was found to be unacceptable: for $\alpha = 0.4$ and $\phi = 0.05$, the value predicted by the Richardson–Zaki formula for the smallest particles can be up to seven times larger than the simulated value! On the other hand, the MLB model works surprisingly well for predicting the settling velocity of the upper tail of the particle size distribution, but not the lower tail. Our simulations confirm that Batchelor's model gives quite accurate predictions for all size classes when $\phi \leq 0.05$, yielding discrepancies of the settling velocities that are within 10 % of the numerical results. The Davis & Gecol model and the MLB model give comparable predictions in our range of volume fractions. Both these models tend to overestimate the hindered settling function of the smaller particles. The discrepancy between the models and the simulation data increases as α or ϕ increases, suggesting that future studies should focus on moderately dense suspensions with a wide size ratio.

Although both models overestimate the settling velocity of the smaller particles, the MLB model gives much more accurate predictions than the Richardson–Zaki correlation. The MLB model is also based on the Richardson–Zaki formula, but in the MLB model the Richardson–Zaki formula is used to estimate the particle–fluid slip velocity, not the absolute settling velocity. For applications where the focus is predicting the sedimentation of larger particles (e.g. separation of large particles from a polydisperse mixture), using the MLB model could be sufficient. For applications where the stratification in different layers needs to be predicted (e.g. in sedimentology; Dorrell & Hogg 2010), using the MLB model will overestimate the fraction of the smaller particles in the sediment region. In particle size fractionation by centrifugation or sedimentation (Bonaccorso *et al.* 2013; Backes *et al.* 2016), using the MLB model could give a wrong prediction of the region where most of the small particles are located, jeopardising the entire size fractionation procedure.

Looking at the main assumptions of the MLB model, re-derived in Appendix A, we can see that the model rests on the assumption that the Stokes drag correction for each size class only depends on the total volume fraction of the suspension. This assumption cannot hold in general, and thus this is the main area of model improvement. Despite our efforts, we have not been able to propose, based on rigorous fluid mechanics arguments, an improvement of the MLB model in which the effect of polydispersity is accounted for in the closure of the fluid–particle velocity slip. Perhaps data for the drag force on polydisperse fixed arrays subject to a uniform flow (van der Hoef, Beetstra & Kuipers 2005; Sarkar, van der Hoef & Kuipers 2009; Yin & Sundaresan 2009; Cheng & Wachs 2023*a*) could be used to suggest improved models. However, one should take into account that uniform flow past a fixed polydisperse array and the average velocity of a polydisperse array subject to known external forces are two different problems. Given the difficulty in coming up with a closure relation valid for all particle sizes, machine learning techniques such as symbolic regression (Zhang & Ma 2020; Cheng & Wachs 2023*b*; El Hasadi & Padding 2023; Wu & Zhang 2023) could be used to incorporate into the MLB model information about the moments of the particle size distribution.
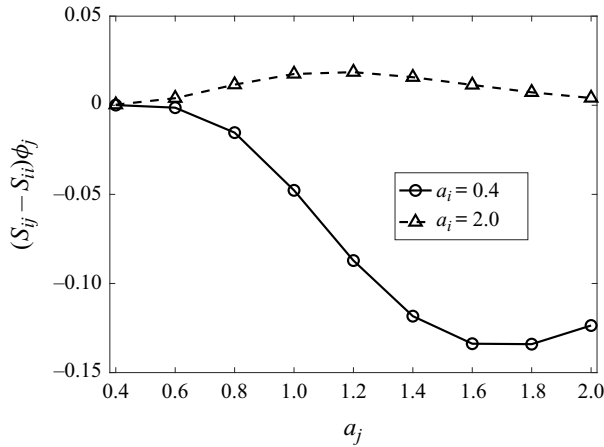
Figure 28. Inter-class interaction term appearing on the right-hand side of (7.1) for $a_i = 0.4$ ('small' particles) and $a_i = 2$ ('large' particles). The particle size distribution corresponds to $\alpha = 0.4$ and $\phi = 0.05$.

The good comparison between Batchelor's model and the simulation data for sufficiently small ϕ enables us to use this analytical model to illustrate why the prediction of the velocity of the small particles is highly dependent on the full particle size distribution, while that of the large particles is not. Equation (2.1) can be rewritten as

$$h_i = 1 + S_{ii}\phi + \sum_{j=1}^{m}(S_{ij} - S_{ii})\phi_j, \tag{7.1}$$

where $S_{ii} = -6.55$ and ϕ is the total volume fraction. The direct influence of the size of particle class j on the hindered settling of particle class i is negligible if $|(S_{ij} - S_{ii})\phi_j| \ll |S_{ii}\phi|$. For $\phi = 0.05$, the magnitude of the intra-class interaction term is $|S_{ii}\phi| = 0.33$. Let us compare this value with the inter-class interaction term for $\phi = 0.05$. In figure 28 $(S_{ij} - S_{ii})\phi_j$ is shown for $a_i = 0.4$ (small particles) and $a_i = 2$ (large particles), for $\alpha = 0.4$. The maximum absolute value of the inter-class interaction term for the small particles is 0.13, not negligible in comparison with 0.33. The maximum value of the inter-class interaction term for the largest particles is instead 18 times smaller than the intra-class interaction term. The question is: in the case of log-normally distributed particles, why is the inter-class interaction term small for the large particles? Is this because the interaction coefficients are small in magnitude? Or because of the distribution of volume fractions?

To reply to these questions, in figure 29(a,b) we show $(S_{ij} - S_{ii})$ and ϕ separately. For completeness, in figure 29(a) $(S_{ij} - S_{ii})$ is shown also for $a_j/a_i \to 0$ (even though the smallest value we consider in our work is 0.2). It is seen that in our log-normal distribution the volume fraction corresponding to the small particles is small in comparison with that of the large particles, and tends to zero as the lower tail of the particle size distribution is approached. The quantity $(S_{ij} - S_{ii})$ is on the other hand not diverging for $a_j/a_i \ll 1$, and is $O(1)$ in this limit. Therefore, specifically for a log-normal particle size distribution the reason why the lower tail has a small influence on the upper tail is that the volume fraction corresponding to the lower tail is comparatively small and is weighted by an interaction term that is not large. For a more general particle size distribution, the situation is more subtle. For example, if the particle size distribution was such that ϕ was comparatively large in the small particle range, one would expect the settling velocity of the largest particles to be more affected by the smallest particles than seen in our simulations. To test
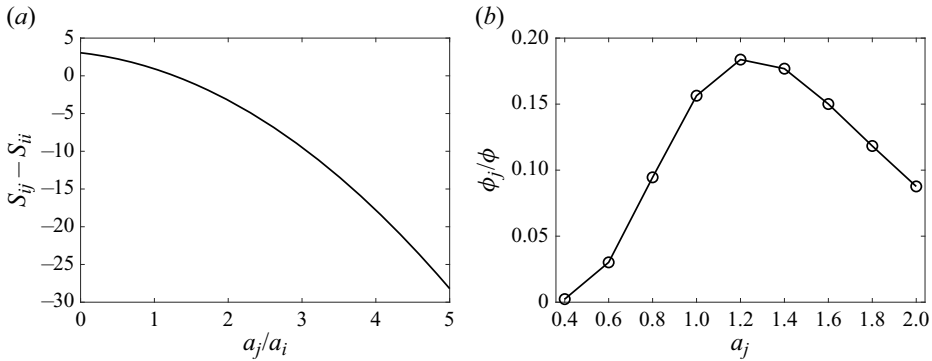
1001 A30-26

Figure 29. (*a*) Interaction coefficients $S_{ij} - S_{ii}$ and (*b*) volume fraction distribution corresponding to the interaction term of figure 28.
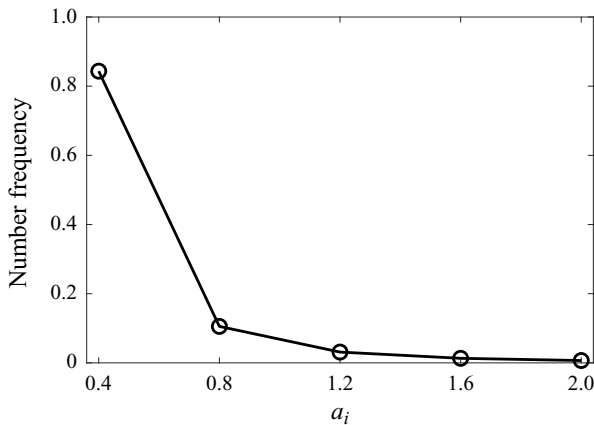

Figure 30. Number-frequency distribution of a polydisperse suspension where all size classes have the same volume fraction.

this hypothesis, we simulated a case where there are five size classes and all size classes have the same volume fraction. The corresponding number-frequency distribution is shown in figure 30. The smallest size class occupies in terms of particle numbers more than 80 % of the total. The normalised average settling velocities from simulations and model predictions are shown in figure 31 for a total volume fraction of 0.03. Batchelor's model gives quite accurate predictions, whereas other models overpredict the hindered settling functions of smaller size classes. The large particles are still relatively uninfluenced by the small particles, even if the volume fraction of the small particles is significantly larger than in the simulations with the log-normal particle size distribution. The reason for this is that while $S_{ij} - S_{ii} \approx 3$ for $a_j/a_i \ll 1$, this $O(1)$ value is still much smaller than the value $|S_{ij} - S_{ii}| \approx 30$ for a_j/a_i close to 5 (see figure 29). In other words, the settling velocity of large particles is directly influenced by the size distribution of particles in neighbouring size classes only. It seems that, from the point of view of the velocity of the large particles, the specific size distribution of the small particles does not matter, only the total volume fraction contribution due to the small particles matters, via the term $S_{ii}\phi$ in (7.1).

The analysis above also gives insights into the condition for which models parametrised on the total volume fraction can be used as a first, practical approximation for the
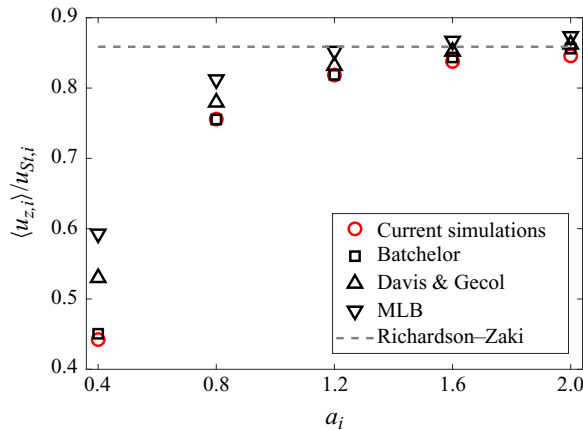
Figure 31. Hindered settling function corresponding to the size distribution of figure 30.

prediction of the settling of a dilute polydisperse suspension. This approximation is reasonable when the inter-class interaction term is comparatively small. This term is small either when $\phi_j \ll 1$ for finite $S_{ij} - S_{ii}$, the case discussed above, or when $|S_{ij} - S_{ii}| \to 0$, the case discussed by Davis & Hassen (1988) (see the value of $S_{ij} - S_{ii}$ for a_j/a_i approaching 1 in figure 28a). If deviations of S_{ij} from S_{ii} are small, then it can be seen from (3.9) that the hindered settling function for $\phi \ll 1$ depends only on the total volume fraction. For a not too dense suspension with a narrow size distribution, the use of the Richardson–Zaki correlation is for example partially justified (note that the exponent $n \simeq 5$ in the Richardson–Zaki correlation is numerically close to $|S_{ii}| = 6.5$; this 'lucky coincidence' was also noted by Davis & Hassen (1988)).

A challenge in the current investigation has been the lack of experimental data with which to compare. Experimental techniques such as X-ray radiography (Dulanjalee *et al.* 2020), magnetic resonance imaging (Boyce *et al.* 2016) or optical experiments with fluorescent particles (Snabre *et al.* 2009) could be used to measure the velocity of a given small particle fraction in a widely polydisperse suspension.

Author ORCIDs.
Heng Li https://orcid.org/0000-0002-9323-4601;
Lorenzo Botto https://orcid.org/0000-0002-7727-5155.

Appendix A. Derivation of the slip velocity closure in the MLB model

A derivation of the MLB model is provided here to highlight the key assumptions of the model, which was too concisely described in the original papers (Lockett & Bassoon 1979; Masliyah 1979). Consider a homogeneous polydisperse suspension with m

particulate classes. The radius and density of the jth class are a_j and ρ_j, respectively, with $j = 1, 2, \ldots, m$. The density and dynamic viscosity of the fluid are ρ_f and μ, respectively. Gravity is in the negative z direction. Due to the differences between the particle and the fluid densities, a macroscopic pressure gradient $\mathrm{d}p/\mathrm{d}z$ along the height of the mixture is needed to balance the excess weight of the particles. This pressure gradient drives the back flow of the fluid during settling of the particles. Corresponding to this pressure gradient, each particle experiences a buoyancy force $F_{\nabla p} = (-\mathrm{d}p/\mathrm{d}z)V_p$, where V_p is the volume of that particle. The total force exerted on each particle by the fluid is given by $F_{\nabla p}$, by the buoyancy force due to the undisturbed hydrostatic pressure gradient and by the drag force due to the relative fluid–particle velocity difference.

The steady-state momentum equation for the fluid phase is

$$\left(-\frac{\mathrm{d}p}{\mathrm{d}z}\right)(1 - \phi) - \sum_{j=1}^{m} f_{d,j} = 0, \tag{A1}$$

where ϕ is the total volume fraction and $f_{d,j}$ is the volumetric drag force density (drag per unit volume) exerted by the jth particle class. The steady-state particle momentum equation for the jth particle class is

$$\left(-\frac{\mathrm{d}p}{\mathrm{d}z}\right)\phi_j + f_{d,j} - (\rho_j - \rho_f)\phi_j g = 0, \tag{A2}$$

where ϕ_j is the volume fraction of the jth class. Using (A1) and (A2) gives

$$\frac{\mathrm{d}p}{\mathrm{d}z} = -\sum_{j=1}^{m}(\rho_j - \rho_f)\phi_j g \tag{A3}$$

and

$$f_{d,j} = (\rho_j - \rho_{susp})\phi_j g, \tag{A4}$$

where $\rho_{susp} = (1 - \phi)\rho_f + \sum_{i=1}^{m} \rho_i \phi_i$ is the density of the suspension (see e.g. Xia *et al.* (2022) for the case $m = 1$). The predictive accuracy of (A4) for small particles immersed in a suspension of larger particles has been put into question (Poletto & Joseph 1995; Rotondi, Di Felice & Pagliai 2015).

To calculate the particle velocity, a constitutive equation relating relative velocity to force must be postulated. The MLB model uses a linear law between the drag force and the slip velocity $u_{slip,j}$ between the jth particle class and the average fluid velocity:

$$f_{d,j} = -\beta_j u_{slip,j}, \tag{A5}$$

where $u_{slip,j}$ is defined as in (5.1). The friction coefficient was calculated as $\beta_j = 9\mu\phi_j C(\phi)/2a_j^2$. The case $C = 1$ corresponds to no influence of neighbouring particles on the drag force exerted on a test particle (the factor ϕ_j is due to the fact that $f_{d,j}$ is a force per unit volume). To model hydrodynamic interactions on the drag force, the MLB model assumes $C(\phi) = (1 - \phi)^{2-n}$, as for a monodisperse case at the same total volume fraction (from the Richardson–Zaki correlation, the slip velocity in the monodisperse case is $u_{slip} = \langle u_p \rangle - \langle u_f \rangle = \langle u_p \rangle/(1 - \phi) = u_{St}(1 - \phi)^{n-1}$; equating (A4) and (A5) using this slip velocity gives $C(\phi) = (1 - \phi)^{2-n}$).

From (A4) and (A5), the slip velocity for the polydispersed case is

$$u_{slip,j} = \frac{2a_j^2}{9\mu}(1-\phi)^{n-2}(\rho_j - \rho_{susp}). \tag{A6}$$

If all the particles have the same density, $\rho_{susp} = (1-\phi)\rho_f + \phi\rho_p$ and $\rho_j - \rho_{susp} = (1-\phi)(\rho_p - \rho_f)$. In this case the slip velocity simplifies to

$$u_{slip,j} = u_{St,j}(1-\phi)^{n-1}, \tag{A7}$$

where $u_{St,j}$ is the Stokes velocity of the jth species. Using the definition of the slip velocity and using mass continuity $\sum_j \phi_j \langle u_j \rangle + (1-\phi)\langle u_f \rangle = 0$ yields (2.3).

It can be seen from the derivation that the main assumptions in the MLB model are embedded in (A4) and (A5).

REFERENCES

ABBAS, M., CLIMENT, E., SIMONIN, O. & MAXEY, M.R. 2006 Dynamics of bidisperse suspensions under Stokes flows: linear shear flow and sedimentation. *Phys. Fluids* **18** (12), 121504.

ABEYNAIKE, A., SEDERMAN, A.J., KHAN, Y., JOHNS, M.L., DAVIDSON, J.F. & MACKLEY, M.R. 2012 The experimental measurement and modelling of sedimentation and creaming for glycerol/biodiesel droplet dispersions. *Chem. Engng Sci.* **79**, 125–137.

AL-NAAFA, M.A. & SELIM, M.S. 1992 Sedimentation of monodisperse and bidisperse hard-sphere colloidal suspensions. *AIChE J.* **38** (10), 1618–1630.

BACKES, C., *et al.* 2016 Production of highly monolayer enriched dispersions of liquid-exfoliated nanosheets by liquid cascade centrifugation. *ACS Nano* **10** (1), 1589–1601.

BATCHELOR, G.K. 1972 Sedimentation in a dilute dispersion of spheres. *J. Fluid Mech.* **52** (2), 245–268.

BATCHELOR, G.K. 1982 Sedimentation in a dilute polydisperse system of interacting spheres. Part 1. General theory. *J. Fluid Mech.* **119**, 379–408.

BATCHELOR, G.K. & JANSE VAN RENSBURG, R.W. 1986 Structure formation in bidisperse sedimentation. *J. Fluid Mech.* **166**, 379–407.

BATCHELOR, G.K. & WEN, C.S. 1982 Sedimentation in a dilute polydisperse system of interacting spheres. Part 2. Numerical results. *J. Fluid Mech.* **124**, 495–528.

BEENAKKER, C.W.J. 1986 Ewald sum of the Rotne–Prager tensor. *J. Chem. Phys.* **85** (3), 1581–1582.

BERRES, S., BÜRGER, R. & TORY, E.M. 2005 Applications of polydisperse sedimentation models. *Chem. Engng J.* **111** (2–3), 105–117.

BONACCORSO, F., ZERBETTO, M., FERRARI, A.C. & AMENDOLA, V. 2013 Sorting nanoparticles by centrifugal fields in clean media. *J. Phys. Chem.* C **117** (25), 13217–13229.

BOYCE, C.M., RICE, N.P., OZEL, A., DAVIDSON, J.F., SEDERMAN, A.J., GLADDEN, L.F., SUNDARESAN, S., DENNIS, J.S. & HOLLAND, D.J. 2016 Magnetic resonance characterization of coupled gas and particle dynamics in a bubbling fluidized bed. *Phys. Rev. Fluids* **1** (7), 074201.

BRADY, J.F. & BOSSIS, G. 1988 Stokesian dynamics. *Annu. Rev. Fluid Mech.* **20** (1), 111–157.

BRADY, J.F. & DURLOFSKY, L.J. 1988 The sedimentation rate of disordered suspensions. *Phys. Fluids* **31** (4), 717–727.

BRADY, J.F., PHILLIPS, R.J., LESTER, J.C. & BOSSIS, G. 1988 Dynamic simulation of hydrodynamically interacting suspensions. *J. Fluid Mech.* **195**, 257–280.

BRZINSKI, T.A. III & Durian, D.J. 2018 Observation of two branches in the hindered settling function at low Reynolds number. *Phys. Rev. Fluids* **3** (12), 124303.

CHEN, H., JIA, X., FAIRWEATHER, M. & HUNTER, T.N. 2023 Characterising the sedimentation of bidisperse colloidal silica using analytical centrifugation. *Adv. Powder Technol.* **34** (2), 103950.

CHENG, Z. & WACHS, A. 2023*a* Hydrodynamic force and torque fluctuations in a random array of polydisperse stationary spheres. *Intl J. Multiphase Flow* **167**, 104524.

CHENG, Z. & WACHS, A. 2023*b* Physics-informed neural network for modeling force and torque fluctuations in a random array of bidisperse spheres. *Intl J. Multiphase Flow* **169**, 104603.

CUNHA, F.R., ABADE, G.C., SOUSA, A.J. & HINCH, E.J. 2002 Modeling and direct simulation of velocity fluctuations and particle-velocity correlations in sedimentation. *J. Fluids Engng* **124** (4), 957–968.

CUTHBERTSON, A., DONG, P., KING, S. & DAVIES, P. 2008 Hindered settling velocity of cohesive/non-cohesive sediment mixtures. *Coast. Engng* **55** (12), 1197–1208.

DAVIS, R.H. & ACRIVOS, A. 1985 Sedimentation of noncolloidal particles at low Reynolds numbers. *Annu. Rev. Fluid Mech.* **17** (1), 91–118.

DAVIS, R.H. & BIRDSELL, K.H. 1988 Hindered settling of semidilute monodisperse and polydisperse suspensions. *AIChE J.* **34** (1), 123–129.

DAVIS, R.H. & GECOL, H. 1994 Hindered settling function with no empirical parameters for polydisperse suspensions. *AIChE J.* **40** (3), 570–575.

DAVIS, R.H. & HASSEN, M.A. 1988 Spreading of the interface at the top of a slightly polydisperse sedimenting suspension. *J. Fluid Mech.* **196**, 107–134.

DI VAIRA, N.J., ŁANIEWSKI-WOŁŁK, Ł., JOHNSON, R.L., AMINOSSADATI, S.M. & LEONARDI, C.R. 2022 Influence of particle polydispersity on bulk migration and size segregation in channel flows. *J. Fluid Mech.* **939**, A30.

DORRELL, R. & HOGG, A.J. 2010 Sedimentation of bidisperse suspensions. *Intl J. Multiphase Flow* **36** (6), 481–490.

DULANJALEE, E., GUILLARD, F., BAKER, J., EINAV, I. & MARKS, B. 2020 Measuring grain size fractions of bidisperse granular materials using X-ray radiography. *Opt. Express* **28** (20), 29202–29211.

EL HASADI, Y.M.F. & PADDING, J.T. 2023 Do logarithmic terms exist in the drag coefficient of a single sphere at high Reynolds numbers? *Chem. Engng Sci.* **265**, 118195.

GONZALEZ, E., APONTE-RIVERA, C. & ZIA, R.N. 2021 Impact of polydispersity and confinement on diffusion in hydrodynamically interacting colloidal suspensions. *J. Fluid Mech.* **925**, A35.

HASE, K.R. & POWELL, R.L. 2001 Calculation of the Ewald summed far-field mobility functions for arbitrarily sized spherical particles in Stokes flow. *Phys. Fluids* **13** (1), 32–44.

HASIMOTO, H. 1959 On the periodic fundamental solutions of the Stokes equations and their application to viscous flow past a cubic array of spheres. *J. Fluid Mech.* **5** (2), 317–328.

HAYAKAWA, H. & ICHIKI, K. 1995 Statistical theory of sedimentation of disordered suspensions. *Phys. Rev. E* **51** (5), R3815.

HE, W., WANG, Q., ZHU, Y., WANG, K., MAO, J., XUE, X. & SHI, Y. 2021 Innovative technology of municipal wastewater treatment for rapid sludge sedimentation and enhancing pollutants removal with nano-material. *Bioresour. Technol.* **324**, 124675.

VAN DER HOEF, M.A., BEETSTRA, R. & KUIPERS, J.A.M. 2005 Lattice–Boltzmann simulations of low-Reynolds-number flow past mono-and bidisperse arrays of spheres: results for the permeability and drag force. *J. Fluid Mech.* **528**, 233–254.

HOWARD, A.A., MAXEY, M.R. & GALLIER, S. 2022 Bidisperse suspension balance model. *Phys. Rev. Fluids* **7** (12), 124301.

KIM, S. & KARRILA, S.J. 2013 *Microhydrodynamics: Principles and Selected Applications*. Butterworth-Heinemann.

LAVRENTEVA, O.M., SMAGIN, I. & NIR, A. 2024 Shear-induced particle migration in viscous suspensions with continuous size distribution. *Phys. Rev. Fluids* **9** (2), 024305.

LOCKETT, M.J. & BASSOON, K.S. 1979 Sedimentation of binary particle mixtures. *Powder Technol.* **24** (1), 1–7.

MALBRANCHE, N., CHAKRABORTY, B. & MORRIS, J.F. 2023 Shear thickening in dense bidisperse suspensions. *J. Rheol.* **67** (1), 91–104.

MASLIYAH, J.H. 1979 Hindered settling in a multi-species particle system. *Chem. Engng Sci.* **34** (9), 1166–1168.

MONCHO-JORDÁ, A., LOUIS, A.A. & PADDING, J.T. 2010 Effects of interparticle attractions on colloidal sedimentation. *Phys. Rev. Lett.* **104** (6), 068301.

NICOLAI, H., HERZHAFT, B., HINCH, E.J., OGER, L. & GUAZZELLI, E. 1995 Particle velocity fluctuations and hydrodynamic self-diffusion of sedimenting non-Brownian spheres. *Phys. Fluids* **7** (1), 12–23.

PADDING, J.T. & LOUIS, A.A. 2004 Hydrodynamic and Brownian fluctuations in sedimenting suspensions. *Phys. Rev. Lett.* **93** (22), 220601.

PAPUGA, K., KASZUBKIEWICZ, J. & KAWAŁKO, D. 2021 Do we have to use suspensions with low concentrations in determination of particle size distribution by sedimentation methods? *Powder Technol.* **389**, 507–521.

PEDNEKAR, S., CHUN, J. & MORRIS, J.F. 2018 Bidisperse and polydisperse suspension rheology at large solid fraction. *J. Rheol.* **62** (2), 513–526.

PEYSSON, Y. & GUAZZELLI, E. 1999 Velocity fluctuations in a bidisperse sedimenting suspension. *Phys. Fluids* **11** (7), 1953–1955.

PHILLIPS, R.J., BRADY, J.F. & BOSSIS, G. 1988 Hydrodynamic transport properties of hard-sphere dispersions. I. Suspensions of freely mobile particles. *Phys. Fluids* **31** (12), 3462–3472.

POLETTO, M. & JOSEPH, D.D. 1995 Effective density and viscosity of a suspension. *J. Rheol.* **39** (2), 323–343.

RETTINGER, C., EIBL, S., RÜDE, U. & VOWINCKEL, B. 2022 Rheology of mobile sediment beds in laminar shear flow: effects of creep and polydispersity. *J. Fluid Mech.* **932**, A1.

REVAY, J.M. & HIGDON, J.J.L. 1992 Numerical simulation of polydisperse sedimentation: equal-sized spheres. *J. Fluid Mech.* **243**, 15–32.

RICHARDSON, J.F.T. & ZAKI, W.N. 1954 Sedimentation and fluidization: part 1. *Trans. Inst. Chem. Engrs* **32**, 35–53.

ROTNE, J. & PRAGER, S. 1969 Variational treatment of hydrodynamic interaction in polymers. *J. Chem. Phys.* **50** (11), 4831–4837.

ROTONDI, M., DI FELICE, R. & PAGLIAI, P. 2015 Validation of fluid–particle interaction force relationships in binary-solid suspensions. *Particuology* **23**, 40–48.

SARKAR, S., VAN DER HOEF, M.A. & KUIPERS, J.A.M. 2009 Fluid–particle interaction from lattice Boltzmann simulations for flow through polydisperse random arrays of spheres. *Chem. Engng Sci.* **64** (11), 2683–2691.

SHAJAHAN, T. & BREUGEM, W. 2023 Inertial effects in sedimenting suspensions of solid spheres in a liquid. *Intl J. Multiphase Flow* **166**, 104498.

SNABRE, P., POULIGNY, B., METAYER, C. & NADAL, F. 2009 Size segregation and particle velocity fluctuations in settling concentrated suspensions. *Rheol. Acta* **48**, 855–870.

SPEARMAN, J. & MANNING, A.J. 2017 On the hindered settling of sand-mud suspensions. *Ocean Dyn.* **67**, 465–483.

VOWINCKEL, B., WITHERS, J., LUZZATTO-FEGIZ, P. & MEIBURG, E. 2019 Settling of cohesive sediment: particle-resolved simulations. *J. Fluid Mech.* **858**, 5–44.

WACHOLDER, E. & SATHER, N.F. 1974 The hydrodynamic interaction of two unequal spheres moving under gravity through quiescent viscous fluid. *J. Fluid Mech.* **65** (3), 417–437.

WANG, M. & BRADY, J.F. 2015 Short-time transport properties of bidisperse suspensions and porous media: a Stokesian dynamics study. *J. Chem. Phys.* **142** (9), 094901.

WILLEN, D.P. & PROSPERETTI, A. 2019 Resolved simulations of sedimenting suspensions of spheres. *Phys. Rev. Fluids* **4** (1), 014304.

WU, C. & ZHANG, Y. 2023 Enhancing the shear-stress-transport turbulence model with symbolic regression: a generalizable and interpretable data-driven approach. *Phys. Rev. Fluids* **8** (8), 084604.

XIA, Y., YU, Z., PAN, D., LIN, Z. & GUO, Y. 2022 Drag model from interface-resolved simulations of particle sedimentation in a periodic domain and vertical turbulent channel flows. *J. Fluid Mech.* **944**, A25.

XUE, B. & SUN, Y. 2003 Modeling of sedimentation of polydisperse spherical beads with a broad size distribution. *Chem. Engng Sci.* **58** (8), 1531–1543.

YAO, Y., CRIDDLE, C.S. & FRINGER, O.B. 2021 The effects of particle clustering on hindered settling in high-concentration particle suspensions. *J. Fluid Mech.* **920**, A40.

YIN, X. & SUNDARESAN, S. 2009 Fluid-particle drag in low-Reynolds-number polydisperse gas–solid suspensions. *AIChE J.* **55** (6), 1352–1368.

ZHANG, J. & MA, W. 2020 Data-driven discovery of governing equations for fluid dynamics based on molecular simulation. *J. Fluid Mech.* **892**, A5.

ZUK, P.J., WAJNRYB, E., MIZERSKI, K.A. & SZYMCZAK, P. 2014 Rotne–Prager–Yamakawa approximation for different-sized particles in application to macromolecular bead models. *J. Fluid Mech.* **741**, R5.